Particle transport and finite-size effects in Lorentz channels with finite horizons

Physica D 472 (2025) 134512

Contents lists available at ScienceDirect

Physica D

journal homepage: www.elsevier.com/locate/physd

Particle transport and finite-size effects in Lorentz channels with finite horizons

Emilio N.M. Cirillo [a], Matteo Colangeli [b], Martin Kröger [c,*], Lamberto Rondoni [d,e]

[a] Dipartimento di Scienze di Base e Applicate per l'Ingegneria, Sapienza Università di Roma, via Antonio Scarpa 16, 00161 Rome, Italy
[b] Dipartimento di Ingegneria e Scienze dell'Informazione e Matematica, Università degli Studi dell'Aquila, Via Vetoio, 67100 L'Aquila, Italy
[c] Magnetism and Interface Physics & Computational Polymer Physics, Department of Materials, ETH Zurich, Leopold-Ruzicka-Weg 4, CH 8093, Zurich, Switzerland
[d] Dipartimento di Scienze Matematiche, Politecnico di Torino, Corso Duca degli Abruzzi 24, Turin, Italy
[e] INFN, Sezione di Torino, Via P. Giuria 1, 10125 Turin, Italy

ARTICLE INFO

Communicated by Liang Huang

Keywords:
Lorentz channel
Finite size effects
Correlated random walk
Passage time
Statistical mechanics

ABSTRACT

Particle transport is investigated in a finite-size realization of the classical Lorentz gas model. We consider point particles moving at constant speed in a 2D rectangular strip of finite length, filled with circular scatterers sitting at the vertices of a triangular lattice. Particles are injected at the left boundary with a prescribed rate, undergo specular reflections when colliding with the scatterers and the horizontal boundaries of the channel, and are finally absorbed at the left or the right boundary. Thanks to the equivalence with give Correlated Random Walks, in the finite horizon case, we show that the inverse probability that a particle exits through the right boundary depends linearly on the number of cells in the channel. A non-monotonic behavior of such probability as a function of the density of scatterers is also discussed and traced back analytically to the geometric features of a single trap. This way, we do not refer to asymptotic quantities and we accurately quantify the finite size effects. Our deterministic model provides a microscopic support for a variety of phenomenological laws, *e.g.* the Darcy's law for porous media and the Ohm's law in electronic transport.

1. Introduction

In 1905, Lorentz published three papers on the motion of electrons in metallic bodies [1–3]. The proposed model consisted of point particles, that do not interact with each other and are scattered by and in thermodynamic equilibrium with the atoms of a lattice at a given temperature T. These works advanced those by Riecke, Drude, and Thomson on the electric conductivity of metals for electricity and heat, the thermoelectric currents, the Thomson-effect, and the Hall effect. Later a simplified model was considered to investigate the relation between Hamiltonian particle systems and irreversibility: a model made of a single point particle, scattered by fixed disks, meant to represent very massive atoms. Such a model is commonly called Lorentz gas, although it substantially differs from Lorentz's original model, because fixed disks do not allow a thermodynamic state to be established [4,5]. Sinai proved the ergodicity of the new model [6], which is thus also called Sinai billiard. It was later proven that the dynamics of the Lorentz gas in this modern sense, changes for the case in which the moving particle is allowed to have infinitely long collisionless trajectories, also called infinite horizon case, and the finite horizon case in which all trajectories go through collisions. In the second case, not only the dynamics are ergodic, but the autocorrelation function of the particle velocity decays exponentially in time and, in the proper macroscopic limit, it turns formally equivalent to a self-diffusion process, corresponding to a random walk, [7–10]. Therefore, this model can be considered in the development of a minimal theory of transport of mass in porous media, or even of electrons in solids [11–14]. In the case of infinite horizon, ergodicity remains, but diffusion turns mildly superdiffusive, with the mean square displacement of the particle growing in time t like $t \ln t$, as proven for periodic systems by Bleher [15]. This model is considered *e.g.* in the realm of anomalous transport in confined media [16].

In this paper we tackle the transport properties of a Lorentz gas model from a rather different standpoint, mostly focusing on finite size effects. Specifically, we consider a 2D Lorentz channel with prescribed finite height and length, and equipped with finite horizon realized by placing sufficiently large circular obstacles with centers at the sites of a triangular lattice. Similar kinds of model have been widely investigated in connection with the thermodynamic formalism of dynamical systems

* Corresponding author.
E-mail addresses: emilio.cirillo@uniroma1.it (E.N.M. Cirillo), matteo.colangeli1@univaq.it (M. Colangeli), mk@mat.ethz.ch (M. Kröger), lamberto.rondoni@polito.it (L. Rondoni).

https://doi.org/10.1016/j.physd.2024.134512
Received 5 September 2024; Received in revised form 11 November 2024; Accepted 19 December 2024
Available online 27 December 2024

and the escape rate technique for the calculation of the self diffusion coefficient [17–19]. Here, we show that if particles are inserted in such a channel with a prescribed rate, the ratio between the backscattered flux and the incoming flux increases with rising number of horizontally repeated elementary cells. The result is a kind of transport that can be associated with a resistance that grows proportionally to the length of the channel, in accord with Ohm's law for electrical conduction or the Darcy's law in porous media. Our numerical results are then mirrored by correlated random walks (CRWs), thanks to suitable symbolic dynamics [10,12,19–21] that, doubling the variables of interest produce Markov processes, applicable as long as correlations decay sufficiently fast [22]. In our work, the CRW is needed to represent the fact that the exponentially fast decay of correlations of position and velocity in chaotic dispersive billiards [23] leads to a diffusion (Wiener) process, only under proper scaling of time and length scales, cf. *e.g.* [7,9,24] and part II of [25]. Such scaling, that amounts to a coarse-graining in space and to averaging over many microscopic times, allows the microscopic dynamics to be accurately represented on macroscopic scales by the macroscopic diffusion equation. The system of interest can then be effectively seen as a macroscopic object observed over macroscopic times. On the other hand, the macroscopic relations do not apply to small systems, such as those investigated here: they must be corrected taking into account finite size effects, because particles cannot explore sufficiently large regions of space for sufficiently long times. Their lifetimes within the system compare with, or are even shorter than the times needed for the decay of correlations [26,27]. Consequently, a CRW turns suitable as a theoretical representation of the billiard dynamics at small scales, and transport laws deviate from their infinite system and infinite time limit.

We show quantitatively how finite size corrections to the macroscopic expressions are perfectly captured by a CRW, and how classical results, such as those of Machta and Zwanzig for the diffusion coefficient in the periodic Lorentz gas [8], can be recovered from our more general expressions. Our approach also reveals that the transition to the macroscopic behavior goes through two variations of scales, over which two kinds of correlations have to decay. The first change of scales leads from the *microscopic* to the *mesoscopic* scales, that justify a Markovian representation of the correlated microscopic dynamics. The second variation of scales leads from the *mesoscopic* Markov process to *macroscopic* diffusion. The microscopic scale is given by the billiard dynamics within a distance of a few traps, that is represented by the CRW. The mesoscopic scale corresponds to the billiard dynamics over a limited number of cells, and is represented by the Markov process for the variables of interest. Note, this is not the one with increased number of variables, used to implement the CRW, but a process that arises from coarse-graining over sufficiently large space and time scales. Finally, the macroscopic scale arises in the infinite size and infinite time limit, and is represented by diffusion. Our approach allows us to accurately describe all these scales; in particular the small ones.

2. The 2D Lorentz channel model

We consider a 2D rectangular channel containing an ordered array of circular scatterers, centered at the vertices of a triangular lattice, see Fig. 1. The channel is obtained as a juxtaposition of $n_x \times n_y$ identical disjoint elementary cells, see Fig. 2. The elementary cell is a rectangle having length $\sqrt{3}h$ and height h, with $h > 0$ a real-valued parameter. A circular scatterer is centered at the center of each cell and four more scatterers, having the shape of a quarter of a circle, are placed at its four corners. All the scatterers have radius s, with $0 \le s \le h/2$, so that they do not overlap. Thus, the scatterers are centered at the sites of a triangular lattice with spacing h and the distance between the boundaries of two scatterers with centers at nearest neighbor sites of such a lattice is $h - 2s$, see Fig. 2. Following [8,13] we introduce the dimensionless *separation* parameter $W = (h - 2s)/s$, which is equal to the ratio between the distance between the boundary of neighboring

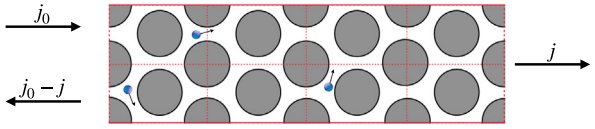

Fig. 1. Schematic description of the periodic 2D linear Lorentz channel with j_0, $j_0 - j$, and j denoting the stationary fluxes of particles. Reflecting (or alternatively, periodic) boundary conditions are imposed along the upper and lower horizontal boundaries of the channel (continuous red lines). The Lorentz channel is partitioned into elementary cells (here, $n_x = 4$ and $n_y = 2$), marked by the dashed red rectangles. Each cell contains two full circular scatterers. Point particles (represented by blue disks) reside in the void space, travel at constant speed v, and undergo elastic collisions with the circular scatterers.

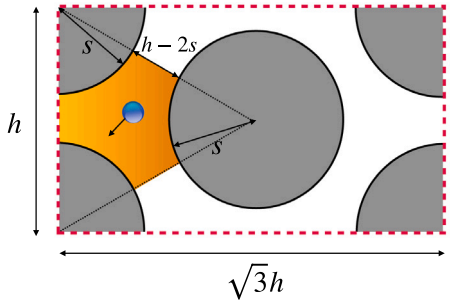

Fig. 2. Schematic representation of the elementary cell of height h, accessed by a point particle (blue disk) in the linear Lorentz channel (Fig. 1) carrying circular scatterers of radius s. The orange shaded area highlights an individual *trapping region* discussed in [8], whose three entries/exits all have identical length $h - 2s$. The finite horizon regime is realized for $\sqrt{3}h < 4s$. A dimensionless gap size is introduced via $W = (h - 2s)/s$.

scatterers and their radius. The length and width of the channel are, respectively, $n_x\sqrt{3}h$ and $n_y h$.

The Lorentz channel is open at its left and right boundaries, with an effective width available to particles entering the channel given by $n_y W s$. Specifically, the channel is thought of as attached at its left boundary to a reservoir injecting particles at a constant rate j_0 with spatial and velocity distribution to be specified in Section 2. Namely, j_0 is the stationary number of particles that, per unit time, enter the channel through the left boundary. Inside the channel the particles do not interact with each other and move at constant speed v colliding elastically with the scatterers. The top and bottom boundaries of the channel are identified, namely, we consider periodic boundary conditions in the vertical y-direction. All quantities to be discussed in this work remain unchanged if we instead use reflecting boundaries for the reason that there is a one-to-one correspondence between periodic and reflecting trajectories. Specifically: (i) the horizontal component of the velocity remains unchanged at the horizontal boundaries; (ii) in the periodic case, a particle hitting the upper boundary would reappear through the bottom boundary with an upward vertical velocity component, whereas in the reflecting case, it would bounce back from the upper boundary with a downward vertical velocity component of the same magnitude. The relevant x-component of a particle's position is thus identical in both versions and the two trajectories are entirely equivalent because the channel is symmetric under reflection about the horizontal median line. Consequently, the statistical properties of interest in this work remain unaffected as well. This way, each trap has three effective exits, even if it appears distributed over two sides of the cell as the trap next to the orange trap in Fig. 2.

We call j the stationary exit rate of particles through the right boundary, see Fig. 1. The main question that we pose in this section is to compute the fraction of particles exiting the channels, namely, the ratio j/j_0. We study the problem in the *finite horizon* regime, *i.e.* $W \in (0, W_c]$, with $W_c = -2 + 4/\sqrt{3} \approx 0.309$, so that a particle cannot

travel through an elementary cell (or Lorentz channel) without hitting an obstacle.

This problem is not new in the literature. For instance, in Fig. 2 of [28], the probability A, referred to as transmission coefficient, is plotted as a function of $2n_x+1$, finding the inverse proportionality $A \propto (2n_x+1)^{-1}$. This is then justified in [28, Section III] through a computation based on a diffusion analogy. In the following years, understanding of the dynamics of the Lorentz gas has improved, in particular about the persistence of motion of particles; moreover, the results highlighted in [28] remain valid asymptotically. Here, we improve that result for what concerns non-asymptotic conditions, profiting from the equivalence of the billiard dynamics with a suitable CRW, that allows a precise estimate of the proportionality coefficient linking A^{-1} to n_x. In particular, we quantify the deviations from proportionality even at small n_x.

We compute numerically the ratio j/j_0 performing the following experiment: we introduce particles through the left end of the channel by choosing at random with uniform probability both the initial position at the left boundary of the channel, and the positive x-component of the velocity. We denote by A the probability that a particle entering the channel from one side exits through the opposing side. Since particles are not trapped in the channel for an infinite time, we have that

$$\frac{j}{j_0} = A. \tag{1}$$

Moreover, the fraction of the incoming particles which, due to backscattering, exit the channel through the left boundary is equal to $1-A$. The probability $A = A(W, n_x)$ depends both on the geometry of the elementary cell, *i.e.* on W, and on the number of longitudinally repeated elementary cells, n_x, while it is by construction unaffected by n_y, h and v. Numerical experiments, shown in Fig. 3, reveal that the ratio between the fraction of reflected and transmitted particles is proportional to n_x with proportionality coefficient depending on W, namely,

$$\frac{j_0 - j}{j} = \frac{1-A}{A} = \beta(W)\, n_x. \tag{2}$$

Fig. 3(**a**), indeed, is a double-logarithmic plot in which the square dots denote the measured values of the quantity $(1-A)/A$ vs. the horizontal number of cells n_x. Each series of data corresponds to a different value of the separation W. The fact that all the straight lines have slope one suggests a simple linear dependency on n_x. The intercept of the lines with the vertical axis gives the value of the proportionality coefficient $\beta(W)$ for different values of W. Fig. 3(**b**), showing a non–constant behavior for $(2n_x+1)A$ vs. $2n_x+1$ illustrates how the proportionality relation $A \propto (2n_x+1)^{-1}$ proposed in Ref. [28] does not hold, unless n_x is sufficiently large. This is in accord with the theory we develop below, which yields relations that apply to any finite n_x. The need for a more general theory is further evidenced by Fig. 4, that reports the measured value of β vs. W. We obtain $\lim_{W\to 0}\beta(W) = 3$, in perfect agreement with the analytic calculations presented in the remainder of the present study.

We wish to discuss the two ingredients of formula (2), that is $\beta(W)$ and the linearity in n_x. To this end we start looking at the crossing probability $\alpha(W)$ for a single trap, from which we derive the crossing probability $a(W) \equiv A(W, n_x = 1)$ for a single cell, and we subsequently apply CRW theory to justify that $(1-A)/A$ is proportional to n_x.

Specifically, to understand particle transport inside a single cell, we first look at the internal structure of a cell, constituted by a sequence of adjacent traps arranged on a triangular array (see Fig. 2).

3. Traps and cells

3.1. Traps

The mean time spent in an individual trapping region (or, for short, *trap*) corresponding to the orange shaded domain portrayed in Fig. 2,

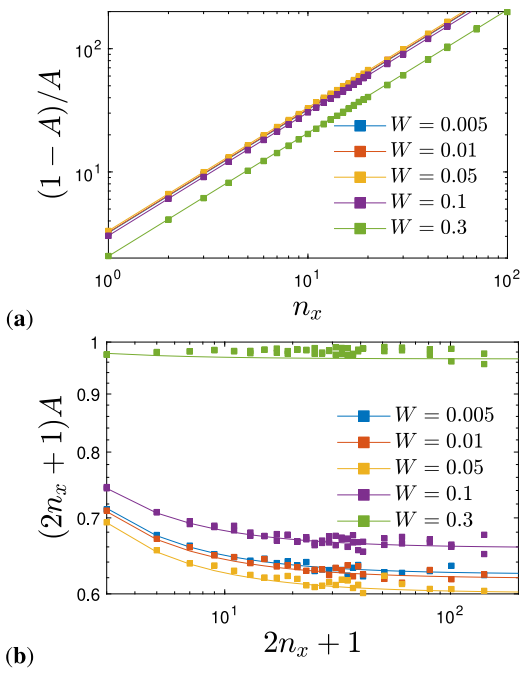

Fig. 3. (**a**) Double-logarithmic plot of the measured $(1-A)/A$ vs. n_x for $W < W_c$, where A denotes the channel crossing probability. Colored squares are obtained numerically, considering 10^6 independent trajectories for each data point. Solid lines have slope one, whereas the intercept on the vertical axis corresponds to $\beta(W)$, cf. Eq. (2). (**b**) Plot of $(2n_x+1)A$ vs. $2n_x+1$. The non–constant behavior, predicted by our theory (solid lines), shows how the $A \propto (2n_x+1)^{-1}$ of [28, Fig. 2] does not hold at n_x smaller than $O(10^2)$.

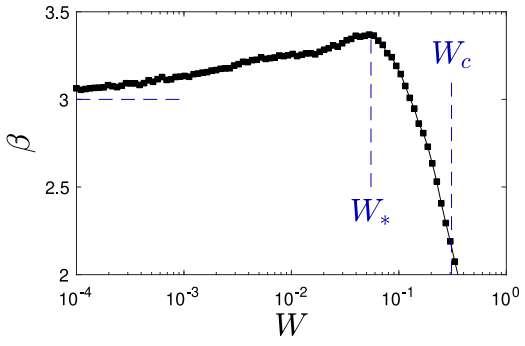

Fig. 4. Semi-logarithmic plot of the measured proportionality coefficient β introduced in (2) vs. W. The black squares are obtained by measuring the intercept with the vertical axis at $n_x = 1$ of the straight lines reported in Fig. 3. The black line is Eq. (18) with $a(W)$ computed numerically. Marked by dashed lines are W_*, the location of the maximum, W_c, the transition to the infinite horizon regime, and the level $\beta = 3$, that is asymptotically approached in the $W \to 0$ limit. Error bars are smaller than symbol sizes.

embedded in an infinite array of cells, is known exactly [8] and given by

$$\tau_{\rm trap} = \frac{\pi s}{6Wv}\left[\frac{\sqrt{3}}{2}(W+2)^2 - \pi\right]. \tag{3}$$

Similarly, the mean number of collisions inside a trap, $c_{\rm trap} = \pi/3W$ had been calculated [8]. The resulting mean time between collisions is therefore $\tau_{\rm trap}/c_{\rm trap}$. These results can be confirmed with high precision upon considering a single trap, if one assumes a uniform velocity distribution inside a trap, or equivalently, a sinusoidal velocity distribution at trap entries. See also the result of our numerical experiment reported in Fig. 5, where a perfect match between numerical data and (3) is detected. For $W \to 0$, $\tau_{\rm trap}$ asymptotically reaches $\tau_{\rm trap} = [2\sqrt{3} - \pi]\pi s/6vW \approx s/6vW$.

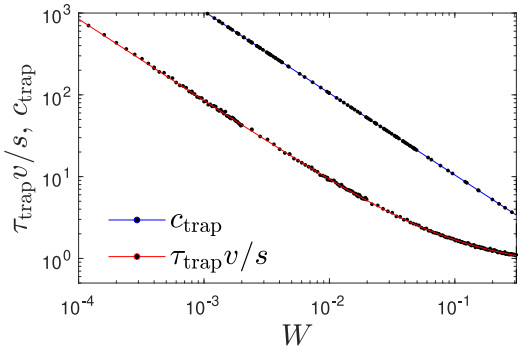

Fig. 5. Measured (black bullets) average number of collisions $c_{\rm trap}$ (blue) and time $\tau_{\rm trap}$ (red) spent in the trapping region versus the dimensionless separation W. The data perfectly agrees with the analytic expressions (solid lines) over the whole W range.

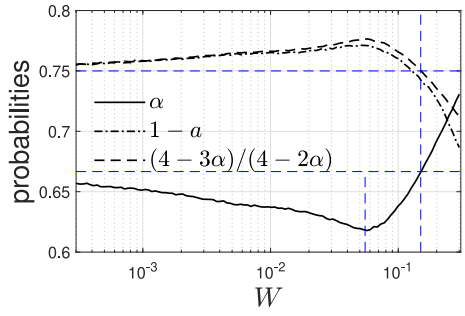

Fig. 6. The measured trap crossing and cell backscatter probabilities α (solid) and $1-a$ (dot-dashed) defined in Sections 3.1 and 3.2 versus W for values up to $W = W_c$. Shown for comparison is the cell backscatter probability $1-a = (4-3\alpha)/(4-2\alpha)$ (dashed) as predicted by Eq. (7). In the limit $W \to 0$ the α and $1-a$ approach $2/3$ and $3/4$, respectively (horizontal dashed blue). Vertical dashed blue lines at $W = W_* \approx 0.05$, where α is minimum, and $W = W_{\rm cf} \approx 0.1547$ where α takes again the value $2/3$.

We therefore focus on a single trap (the orange shaded region in Fig. 2). The figure shows that a trap is connected to other adjacent traps through three gates, each of length $g = h-2s$. A classical question concerns the estimate of the probability that a particle crosses the trap and eventually exits the trap through one of the two doors opposite to the entrance door. This is a function of the dimensionless parameter W, denoted as $\alpha(W)$, called in the sequel *trap crossing probability*. Note that the information about the crossing probability in a single trap does not say anything yet about the probability to pass a cell or a channel along the horizontal direction. This problem is deferred to the next section.

Since we are not able to derive $\alpha(W)$ analytically without imposing any approximations, we determine it numerically. We consider a statistically large number 10^9 of particles entering a trap through the left door, at a vertical coordinate chosen uniformly at random $\in [-g/2, g/2]$ and equipped with a random velocity towards the interior of the trap, such that the horizontal component of the particle velocity is uniformly distributed in the interval $[0, v]$. This ensures a sinusoidal velocity distribution at the trap entry. We follow the collision dynamics of each particle using analytic expressions that derive from the simple geometry of a trap, until it exits the trap through one of the doors, *i.e.* until its position exceeds the distance $s\sqrt{(1+W+W^2)/3}$ from the trap center. We then measure the fraction of particles exiting the trap through one of the doors opposite to the entrance door, and regard this ratio as a meaningful, and high precision estimate of the crossing probability $\alpha(W)$. The measured α versus W is reported by the solid black line in Fig. 6 (the dashed lines will be discussed in Section 3.2). We find that α approaches $2/3$ for $W \to 0$, decreases with increasing W until $W_* \approx 0.05$, where $\alpha(W_*) \approx 5/8$. At larger W the α monotonically increases and approaches $\alpha(W_c) \approx 3/4$ for $W = W_c$.

Specifically, we consider $\alpha(W)$ as the sum of the crossing probabilities α_c resulting from $c \in \mathbb{N}$ collisions against the circular scatterers inside the trap:

$$\alpha(W) = \sum_{c=1}^{\infty} \alpha_c(W). \tag{4}$$

The results of our numerical experiment are reported in Fig. 7, which shows the numerical estimate of the partial sums $\sum_{c=1}^{C} \alpha_c(W)$ for different values of W and $C \in \mathbb{N}$. We observe that the sinusoidal distribution of velocity angles with respect to the channel entries and exits is conserved within measurement precision for $W \ll W_c$, and for larger W only if the contributions from the three exits are added. This means that the sinusoidal distribution is not a strictly invariant entry-exit distribution for all W, if a single trap is considered.

Apart from the crossing probability and mean trap residence time $\tau_{\rm trap}$ one may ask about the mean time $\tau_{\rm trap}^{\hookleftarrow}$ spent in a trap by a particle that exits the trap through the gate through which it entered (or just *mean trap backscattering time*), and the mean time $\tau_{\rm trap}^{\hookrightarrow}$ spent in a trap by a particle that exits the trap through one of the two remaining gates (or *mean trap crossing time*). These times can be measured, are very comparable for $W \ll W_c$ (Fig. 8), and they can be guessed from α and W upon assuming that a particle exits a trap on average within a time interval that is inversely proportional to the corresponding crossing probability (the realization or non-realization of a crossing depends solely on the initial position and velocity of the particle, the exit probability is inversely proportional to the number of collisions required to reach a gap, while the mean time between collisions is insensitive to the exiting gap, i.e., $\tau_{\rm trap}^{\hookrightarrow} \propto 2/\alpha$ and $\tau_{\rm trap}^{\hookleftarrow} \propto (1-\alpha)^{-1}$ with a common factor of proportionality). Since the mean trap residence time, Eq. (3), can also be expressed in terms of $\tau_{\rm trap}^{\hookleftarrow}$ and $\tau_{\rm trap}^{\hookrightarrow}$ in light of the identity $\tau_{\rm trap} = \alpha\tau_{\rm trap}^{\hookrightarrow} + (1-\alpha)\tau_{\rm trap}^{\hookleftarrow}$, we obtain the factor of proportionality $\tau_{\rm trap}/3$ and thus obtain, for $W \ll W_c$, the following expressions:

$$\tau_{\rm trap}^{\hookrightarrow} = \frac{2\tau_{\rm trap}}{3\alpha}, \qquad \tau_{\rm trap}^{\hookleftarrow} = \frac{\tau_{\rm trap}}{3(1-\alpha)}. \tag{5}$$

These formulae descend from the defocusing effect of particles collisions with scatterers, that implies an exponential decay of correlations (statistical effect concerning a coarse-grained description), and lead to a uniform distribution in phase space at long times. Therefore, although a given particle never forgets its initial condition, collections of particles statistically rapidly lose memory of their past, as the number of their collisions grows. The mean number of collisions in a channel is found to obey: $c_{\rm channel} = c_{\rm trap}\tau_{\rm channel}/\tau_{\rm trap} = (\pi/3\ W)\tau_{\rm channel}/\tau_{\rm trap}$ with $\tau_{\rm channel}$ from Eq. (15) and $\tau_{\rm cell}^{\hookleftarrow}$ and $\tau_{\rm cell}^{\hookrightarrow}$ from Eq. (9). Thus, small W implies $\tau_{\rm trap}$ large, and decorrelation within a small distance from the initial position of the particles. In such a case, the residence time does not depend on the gap from which a particle exits the trap, and one obtains $\tau_{\rm trap}^{\hookrightarrow} \approx \tau_{\rm trap}^{\hookleftarrow}$ with α approaching $2/3$ for W shrinking to 0. When the gap is not small, particles leave the trap before the statistical loss of memory has taken place, and a correction is introduced through the numerically computed trap crossing probability α. Indeed, one such parameter suffices, because the number N of particles entering the trap splits as a sum of those exiting from the two right gaps $N^{\hookrightarrow}$, and those exiting from the gap on the left $N^{\hookleftarrow}$, $N = N^{\hookrightarrow} + N^{\hookleftarrow}$, so it suffices to correct one of the two. Eq. (5) also implies $\tau_{\rm trap}^{\hookrightarrow}/\tau_{\rm trap}^{\hookleftarrow} = 2(1-\alpha)/\alpha$ (Fig. 8). The non-obvious non-monotonic behavior of the trap crossing probability with respect to W is thus also reflected by a non-monotonic behavior of the trap crossing and trap backscattering times. For $\alpha = 2/3$, which occurs both in the limit of $W \to 0$ and for some $W \in [W_*, W_c]$, the two conditional residence times are identical.

3.2. Cells

We now shift our focus on the quantity $a(W)$, that is the probability that a particle exits a cell through the vertical (red dashed) exit of the trap numbered as 4, in Fig. 9, provided it entered the cell through

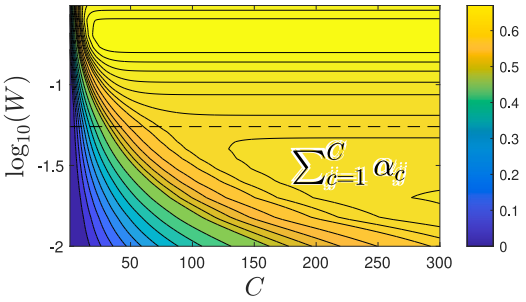

Fig. 7. Property of a single trap. Plot of $\sum_{c=1}^{C} \alpha_c(W)$, the trap crossing probability after C collisions, versus number of collisions C and dimensionless gap size W. Shown is only the regime up to $C = 300$ collisions. The dashed horizontal line marks $W = W_*$. With increasing C the values on the outermost right vertical strip approach $a(W)$ by definition. As visible, the local minimum in $a(W)$ is caused by trajectories with $C \gg 100$ collisions. As we demonstrate analytically, this local minimum translates into the local maximum of β, c.f. Fig. 4.

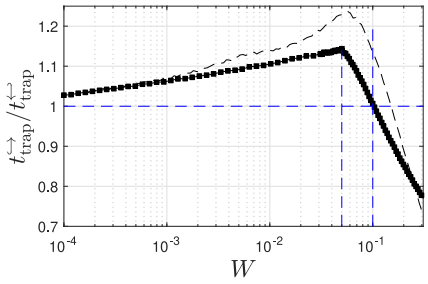

Fig. 8. Ratio $\tau^{\leftrightarrow}_{\rm trap}/\tau^{\leftarrow}_{\rm trap}$ versus W (black bullets) obtained by direct numerical simulation (10^6 trap trajectories for each W). The maximum is located at $W = W_*$. The 2nd vertical blue dashed line is at $W = 0.1$, where $\tau^{\leftrightarrow}_{\rm trap}/\tau^{\leftarrow}_{\rm trap} = 1$ re-achieves its value at $W \to 0$. The non-monotonous behavior of this ratio with respect to W takes over to the non-monotonous behavior of the cell crossing probability a via Eq. (5), and to the non-monotonous behavior of β (Fig. 4) via Eq. (18). Errors comparable with symbol sizes. The dashed black line is $2(1-\alpha)/\alpha$ with the measured α provided by Fig. 6. Eq. (5) holds exactly at small W, and qualitatively also at large $W \simeq W_c$. Even positions of the maxima follow from Eq. (5).

the vertical (red dashed) entry of the trap numbered as 1. Henceforth, $a(W)$ will be referred to, for short, as the *cell crossing probability*. This probability can be calculated numerically following the above approach for a single trap. Under the assumption that the velocity distribution (with respect to the trap-trap gate normals) is invariant, $a(W)$ can be estimated analytically in terms of $\alpha(W)$ using various approaches. One of them, which is particularly easy to follow, while it is not the most compact, is presented next.

First we note that a Markov process can be used to efficiently implement a CRW, if its correlations decay exponentially fast [22]. Then we observe that the elementary cell with vertical periodic (or reflecting) boundary condition is a sequence of four elementary traps that are labeled as T1, T2, T3, T4 from the left to the right, see Fig. 9. The traps T1 and T2 are mutually connected via two gates and so it is also for traps T3 and T4. On the other hand the traps T2 and T3 communicate via a single passage. Thus, retaining the notation of Section 3.1, the motion of a particle entering the cell through the left entrance, namely, through the vertical (red dashed) door of trap T1, can be described via α, i.e. the known crossing probability in a trap. As correlations decay sufficiently fast, compared to the characteristic times of the dynamics in a cell, we may implement the CRW of our interest as a nine state Markov chain on 0,1, … ,8 with 0 and 8 the absorbing states and the states 1, 3, 5, 7 representing the traps T1, T2, T3, and T4 in which the particle entered respectively from traps T0, T1, T2, and T3. On the other hand, the states 2, 4, and 6 represent the traps T1, T2, and T3 in which the particle entered respectively from traps T2,

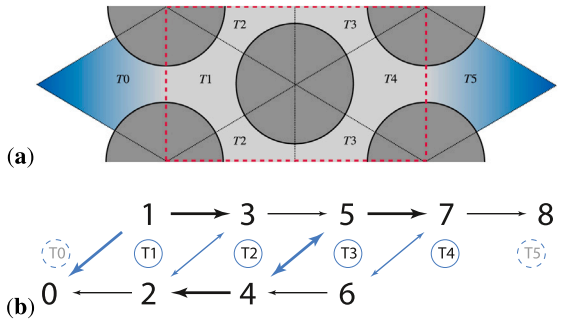

Fig. 9. (**a**) Symbolic representation of a single cell with 4 disjoint communicating traps, under vertical periodic, or reflecting boundary conditions. The traps are numbered from T1 to T4 moving from left to right, blue traps T0 and T5 are located outside the cell. The statistics for the cell crossing probability are unaffected by the choice of boundary condition, because they do not affect the horizontal component of the particle's velocity. (**b**) This system is captured by a 9 states chain, as described in Section 3.2. Absorbing states 0 (trap T0) and 8 (trap T5) are next to traps T1 and T4, respectively. Black arrows mark forward jumps, while blue arrows mark backward jumps, the thickness of arrows is proportional to the jump probability. The connected tree shown in (b) corresponds directly to the transition matrix written down in Eq. (6).

T3, and T4. In light of Fig. 9, the non-zero transition probabilities Q_{ji} between states j and i, can then be defined as follows:

$$\begin{aligned} Q_{13} &= 1 - Q_{10} = \alpha, \\ Q_{20} &= 1 - Q_{23} = \alpha/2, \\ Q_{35} &= 1 - Q_{32} = \alpha/2, \\ Q_{42} &= 1 - Q_{45} = \alpha, \\ Q_{57} &= 1 - Q_{54} = \alpha, \\ Q_{64} &= 1 - Q_{67} = \alpha/2, \\ Q_{78} &= 1 - Q_{76} = \alpha/2. \end{aligned} \tag{6}$$

The probability that a chain that started at state 1 reaches state 8 (trap T5) before state 0 (trap T0) is given by $N_{17}Q_{78}$ where $\mathbf{N}$ is the fundamental matrix, namely, the inverse of $\mathbb{I} - \mathbf{Q}$, where $\mathbf{Q}$ is the 7×7 transition matrix among the transient states, whose non-zero components $Q_{ji} > 0$ are given in Eq. (6). Probabilities to the adsorbing states 0 and 8 hence do not appear in $\mathbf{Q}$ but are listed to highlight the fact that they follow from the conservation of sums of transition probabilities and because they are required for the calculation of residence times and crossing probabilities in the sequel. We then obtain, via matrix inversion,

$$a = N_{17}Q_{78} = \frac{\alpha}{2(2-\alpha)}, \tag{7}$$

with the $\alpha(W)$ studied in the preceding subsection. Accordingly, a monotonically increases with increasing α. If $W \ll W_c$, we recall that α approaches $\alpha = 2/3$. The cell crossing probability a therefore approaches $1/4 = 0.25$ in this limit (Fig. 6). Importantly, Eq. (7) implies that $a \leq 1/2$, because $\alpha \in [0, 1]$ is a probability. Using the foregoing characteristic values for α, we see that $a(W)$ is non-monotonous as well, with $a(W_*) \approx 5/22 \approx 0.223 < 0.25$ and $a(W_c) \approx 3/10 \approx 0.333 > 0.25$. We point out that the estimate (7) allows to capture quantitatively the value of a only for sufficiently small values of W; in particular the match is perfect (Tables 1, 2) in the finite horizon regime that we address in this paper.

Using the conjectured Markov chain we have access not only to the crossing probability a but also to the mean residence time in a cell, $\tau_{\rm cell}$, the mean conditional residence times $\tau^{\leftrightarrow}_{\rm cell}$ and $\tau^{\leftarrow}_{\rm cell}$, to traverse and to backscatter from a cell. The calculation is available in Appendix A. We obtain

$$\tau_{\rm cell} = 6\tau^{\leftarrow}_{\rm cell} + 4\alpha(\tau^{\leftrightarrow}_{\rm cell} - \tau^{\leftarrow}_{\rm cell}),$$

$$\begin{aligned}\tau_{\text{cell}}^{\hookrightarrow} &= \frac{3}{2}(4-\alpha)\tau_{\text{trap}}^{\hookrightarrow} + \left(\frac{32}{\alpha} + 6\alpha - 33 + \frac{2}{2-\alpha}\right)\frac{\tau_{\text{trap}}^{\hookleftarrow}}{4},\\ \tau_{\text{cell}}^{\hookleftarrow} &= \frac{(20-13\alpha)\alpha}{8-6\alpha}\tau_{\text{trap}}^{\hookrightarrow}\\ &\quad + \frac{1}{36}\left[133 - 78\alpha + \frac{18}{2-\alpha} + \frac{8}{4-3\alpha}\right]\tau_{\text{trap}}^{\hookleftarrow}.\end{aligned} \tag{8}$$

Using Eq. (5), Eq. (8) simplifies to

$$\begin{aligned}\tau_{\text{cell}}^{\hookrightarrow} &= \frac{160 - 3\alpha(88 - \alpha(43-6\alpha))}{12(2-\alpha)(1-\alpha)\alpha}\tau_{\text{trap}},\\ \tau_{\text{cell}}^{\hookleftarrow} &= \frac{288 - \alpha[568 - \alpha(367-78\alpha)]}{12(2-\alpha)(1-\alpha)(4-3\alpha)}\tau_{\text{trap}},\\ \tau_{\text{cell}} &= \frac{2(7-6\alpha)}{3(1-\alpha)}\tau_{\text{trap}}.\end{aligned} \tag{9}$$

For $\tau_{\text{trap}}^{\hookleftarrow} = \tau_{\text{trap}}^{\hookrightarrow} = \tau_{\text{trap}}$, and thus, consistently, $\alpha = 2/3$, we obtain $\tau_{\text{cell}} = 6\tau_{\text{trap}}$ with τ_{trap} given by Eq. (3), which is the case in which correlations vanish. This demonstrates, as a by-result, under which circumstances Machta and Zwanzig's phase-space and area arguments towards the calculation of τ_{trap} can be extended to cells and channels. This extension is worked out in Appendix A.

4. The channel

Instead of extending the above 9 states model for a single cell to a $1 + 8n_x$ model for a connected linear, horizontal sequence of n_x cells, we now coarse-grain further our description, and look at the motion of the particles in the channel as a superposition of independent random walks between adjacent cells. This is possible because the entry and exit of the single cell are both vertical, with identical gap size. At variance with previous approaches such as [28], we have to introduce correlations in the jumps, because we just found that the cell crossing probability $a \neq 1/2$. A classical random walk approach therefore does not apply, at any W. It is furthermore important to stress, that $a \neq 1/2$ does not imply that there is any drift. Therefore, we now rely on the theory of CRWs, that allows us to calculate the channel crossing probability in Section 4.1. In Section 4.2 we obtain the channel residence times, while Section 4.3 bridges the gap between these calculations and the problem formulated in Section 2, namely, a microscopically motivated expression for $\beta(W)$. The calculation of the mean square displacement of particles and their diffusion coefficient, based on the CRW approach, is developed in Section 5.

4.1. Correlated Random Walk (CRW)

In this section we provide an interpretation of the numerical results reported in Fig. 3 based on an analogy between our billiard model and a CRW [29]. In particular, we are going to recover observation (2), which is reported as well in Fig. 3 and that matches perfectly with the numerical results.

Indeed, looking at the motion of a particle in the linear Lorentz channel as a motion between neighboring cells, we describe it as a one-dimensional CRW between adjacent cells. One may imagine fixing $n_y = 1$, and imposing periodic boundary conditions along the vertical direction, as the motion in horizontal direction is neither affected by n_y nor by the choice of boundary condition. To this end we consider the fictitious lattice $\{0, 1, \dots, n_x, n_x + 1\}$, with the sites from 1 to n_x representing the cells of the Lorentz channel and the sites 0 and $n_x + 1$ representing the left and right exits. Next, we introduce a random walker that performs a CRW on this lattice in which a denotes the probability to preserve the direction of motion of the random walker, whereas $1 - a$ is the probability to reverse it (i.e. to backscatter). The sites 0 and $n_x + 1$ are absorbing.

The problem we want to solve is the following: for a walker starting at site 1 and moving in the positive direction, let us compute the probability that it reaches the site $n_x + 1$ before reaching the site 0. To do this we denote, respectively, by $p_k^{\hookrightarrow}$ and $p_k^{\hookleftarrow}$ the yet unknown probabilities that a particle initially in cell k reaches cell 0, conditional on its first step being respectively to the right ($\hookrightarrow$) or to the left ($\hookleftarrow$) cell. We obtain

$$\begin{pmatrix} p_{k-1}^{\hookrightarrow} \\ p_{k+1}^{\hookleftarrow} \end{pmatrix} = \begin{pmatrix} a & 1-a \\ 1-a & a \end{pmatrix}\begin{pmatrix} p_k^{\hookrightarrow} \\ p_k^{\hookleftarrow} \end{pmatrix}, \quad k = 2, \dots, n_x. \tag{10}$$

This recursive Eq. (10) is solved by

$$\begin{aligned} p_k^{\hookrightarrow} &= c_1 + c_2 k,\\ p_k^{\hookleftarrow} &= c_1 + c_2\left(k - \frac{1}{1-a}\right),\end{aligned} \tag{11}$$

with boundary values $p_1^{\hookleftarrow} = 1$ and $p_{n_x}^{\hookrightarrow} = 0$, which imply

$$c_1 = \frac{n_x(1-a)}{a + n_x(1-a)}, \qquad c_2 = -\frac{1-a}{a + n_x(1-a)}, \tag{12}$$

yielding

$$p_k^{\hookrightarrow} = \frac{(1-a)(n_x - k)}{a + (1-a)n_x}, \qquad p_k^{\hookleftarrow} = \frac{1 + (1-a)(n_x - k)}{a + (1-a)n_x}. \tag{13}$$

Thus, the probability $A(W, n_x)$ that the correlated random walkers start at $k = 1$ and exit at $k = n_x + 1$, after eventually moving forward and backwards inside the channel with respect to the x-axis, attains the form:

$$\begin{aligned} A(W, n_x) &= 1 - [a p_1^{\hookrightarrow} + (1-a)p_1^{\hookleftarrow}]\\ &= \frac{a}{a + (1-a)n_x}.\end{aligned} \tag{14}$$

This shows that the channel crossing probability A cannot be decomposed into two multiplicative contributions that depend solely on n_x or W. In any event, using Eq. (7), it can alternatively be expressed in terms of the trap property α, revealing that A exhibits a minimum with respect to W.

4.2. Channel residence times

For the cell we had calculated the mean residence time, mean crossing and backscattering times starting from the transition matrix $\mathbf{Q}$ that arose from the 9 states model shown in Fig. 9. This strategy can be adopted for the channel upon replacing the hexagonal arrangement of four traps by a linear arrangement of n_x cells. On one hand the problem is simpler, because the linear arrangement eliminates the need for arrows with different thickness in Fig. 9, on the other hand it is more difficult, because n_x is arbitrary. The $2n_x \times 2n_x$ transition matrix for the channel with n_x cells is given by Eq. (B.2). The problem of calculating the channel residence time τ_{channel}, channel crossing time $\tau_{\text{channel}}^{\hookrightarrow}$, and channel backscatter time $\tau_{\text{channel}}^{\hookleftarrow}$ is worked out in Appendix B using the discrete-time approach.

In short, we obtain explicit expressions for $\tau_{\text{channel}}^{\hookrightarrow}$ and $\tau_{\text{channel}}^{\hookleftarrow}$ in terms of n_x, $\tau_{\text{cell}}^{\hookrightarrow}$, $\tau_{\text{cell}}^{\hookleftarrow}$, and a (or α), stated in Eqs. (B.5) and (B.6). For $n_x = 1$ these expressions reduce to $\tau_{\text{cell}}^{\hookrightarrow}$ and $\tau_{\text{cell}}^{\hookleftarrow}$, as expected. For the channel residence time we obtain

$$\begin{aligned}\tau_{\text{channel}} &= A\tau_{\text{channel}}^{\hookrightarrow} + (1-A)\tau_{\text{channel}}^{\hookleftarrow}\\ &= [a\tau_{\text{cell}}^{\hookrightarrow} + (1-a)\tau_{\text{cell}}^{\hookleftarrow}]n_x,\end{aligned} \tag{15}$$

with A from Eq. (14) or a from Eq. (7). Moreover, Eqs. (B.5) and (B.6) imply that the mean channel crossing time significantly exceeds the mean channel backscattering time by the following amount

$$\frac{\tau_{\text{channel}}^{\hookrightarrow}}{\tau_{\text{channel}}^{\hookleftarrow}} = \frac{(1-a)n_x}{2a}, \qquad (n_x \gg 1) \tag{16}$$

which reduces to $\tau_{\text{cell}}^{\hookrightarrow}/\tau_{\text{cell}}^{\hookleftarrow}$ for $n_x = 1$, with $\tau_{\text{cell}}^{\hookrightarrow}$ and $\tau_{\text{cell}}^{\hookleftarrow}$ given in terms of α and $\tau_{\text{trap}}^{\hookrightarrow}$ and $\tau_{\text{trap}}^{\hookleftarrow}$ by Eq. (8). While the particle can go back and forth through the channel, the mean time to cross a channel is therefore large compared with the backscattering time, and also large compared with the residence time in a channel, when the length of the channel grows. Fig. 10 shows the distribution of residence times, crossing times and backscattering times, as functions of the dimensionless time variable tv/h, for (a) the trap, (b) the cell, and (c) the channel with an assigned

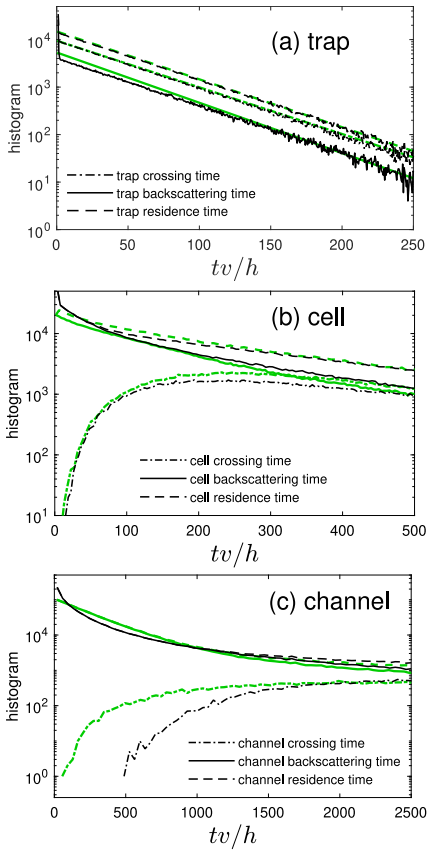

Fig. 10. (**a**) Single trap, (**b**) single cell, $n_x = 1$, (**c**) channel with $n_x = 4$, at $W = 0.002 \ll W_c$. Numerical results for the Lorentz trap, cell and channel marked in black. While the conditional (crossing/backscattering) and unconditional residence times in traps are mono-exponentially distributed, for cells and channels the situation is different at short times; asymptotically their distributions are exponential as well. In longer channels, the histograms follow the n_x trend depicted here. By definition, the histogram of residence times is the sum of the other two histograms. While the distributions are very different in the three cases, their first moments are captured by the analytic approaches, c.f., Tables 1 and 2 for a comparison at $W = 0.002$ and $W = 0.15$, respectively. The green lines result from a continuous-time random walk model, where particles hop between states: For the cell in panel (b), we model the histograms of exit times upon assuming that the exit event times are uncorrelated, i.e., we consider a large number of realizations of particles, that start in trap T1, and choose for each trap-trap crossing between traps Ti and Tj, which is realized with probability Q_{ij}, a random time increment $\Delta\tau = \tau_{\text{trap}}\xi/2Q_{ij}$ with ξ an exponentially distributed random number with unit mean. The choice of Δt ensures that the mean trap residence time is τ_{trap}. Similarly for the channel in (c). Panel (a) for traps shows mono-exponential histograms with their means τ_{trap}, $\tau^{\hookrightarrow}_{\text{trap}}$, and $\tau^{\hookleftarrow}_{\text{trap}}$ given by Eq. (5) with Eq. (3).

finite length, at a relatively small W. As directly visible for the trap, expected for our setup with finite horizon, the distributions for the cell and the channel exhibit exponential tails implying that any moment of arbitrary order of such distributions is finite. The exponential as opposed to algebraic decay furthermore supports the applicability of a CRW, as the two issues are connected due to the chaotic nature of the cell [19,30].

In full analogy with the case of a single cell, the channel residence time $\tau_{\text{channel}} = 6n_x\tau_{\text{trap}}$ that one estimates using Machta and Zwanzig's approach (see Appendix B), is identical with the exact result (15) provided $\tau^{\hookrightarrow}_{\text{cell}} = \tau^{\hookleftarrow}_{\text{cell}} = \tau_{\text{cell}}$. In that case the channel residence time reduces to $\tau_{\text{channel}} = 6n_x\tau_{\text{trap}}$ with τ_{trap} from Eq. (3), so that a particle exits the channel after $2\pi n_x/W$ collisions, on average. We know however from Section 3.2 that $\tau^{\hookrightarrow}_{\text{cell}}$ and $\tau^{\hookleftarrow}_{\text{cell}}$ are usually very different.

Table 1
Comparison between 2D Lorentz channel and analytical predictions for the case selected in Fig. 10, at $W = 0.002$. This table verifies the calculations done in Sections 3, 4 and Appendices A and B. The values of the residence, crossing and backscattering times in cells and channels have all been rounded to their nearest integer. For a larger $W = 0.15$ see Table 2.

Model	α	$\tau^{\hookrightarrow}_{\text{trap}}$	$\tau^{\hookleftarrow}_{\text{trap}}$	τ_{trap}
2D Lorentz trap	0.65	44.27	41.00	43.13
Eqs. (3), (5), (C.2)	0.66	44.17	41.03	43.08
Model	a	$\tau^{\hookrightarrow}_{\text{cell}}$	$\tau^{\hookleftarrow}_{\text{cell}}$	τ_{cell}
2D Lorentz ($n_x = 1$)	0.24	452	197	258
Eqs. (7), (8)	0.24	445	195	255
Model	A	$\tau^{\hookrightarrow}_{\text{channel}}$	$\tau^{\hookleftarrow}_{\text{channel}}$	τ_{channel}
2D Lorentz ($n_x = 4$)	0.073	5065	716	1035
Eqs. (14), (B.5), (B.6)	0.074	5045	716	1037

Table 2
Same as Table 1 for $W = 0.15$.

Model	α	$\tau^{\hookrightarrow}_{\text{trap}}$	$\tau^{\hookleftarrow}_{\text{trap}}$	τ_{trap}
2D Lorentz trap	0.69	1.36	1.49	1.40
Eqs. (3), (5), (C.2)	0.69	1.35	1.50	1.40
Model	a	$\tau^{\hookrightarrow}_{\text{cell}}$	$\tau^{\hookleftarrow}_{\text{cell}}$	τ_{cell}
2D Lorentz ($n_x = 1$)	0.26	13.87	6.50	8.39
Eqs. (7), (8)	0.26	13.87	6.60	8.52
Model	A	$\tau^{\hookrightarrow}_{\text{channel}}$	$\tau^{\hookleftarrow}_{\text{channel}}$	τ_{channel}
2D Lorentz ($n_x = 4$)	0.081	150.9	23.3	33.6
Eqs. (14), (B.5), (B.6)	0.081	148.9	23.5	33.6

4.3. Back to the billiard dynamics

We can finally turn back to the point of departure, namely the particle dynamics in the Lorentz channel of Section 2. Inserting Eq. (14) into Eq. (2) we find

$$\frac{1-A}{A} = \left(\frac{1-a}{a}\right) n_x, \tag{17}$$

where $a = a(W)$ had already been expressed in terms of the trap crossing probability $\alpha(W)$ in Eq. (7), Therefore, through Eq. (17), we have hereby shown that the coefficient $\beta(W)$ in Eq. (2) does not depend on n_x. It can be expressed in terms of the cell crossing probability $a(W)$, or also the trap crossing probability $\alpha(W)$

$$\beta(W) = \frac{1}{a(W)} - 1 = \frac{4}{\alpha(W)} - 3, \tag{18}$$

and one has $A(W, n_x) = [1 + \beta(W)n_x]^{-1}$ as well as $a(W) = A(W, 1)$. In the limit of small W, we therefore derived

$$\lim_{W\to 0} \beta(W) = 3, \qquad \lim_{W\to 0} A(W, n_x) = \frac{1}{1+3n_x}. \tag{19}$$

We stress that the CRW works well as a tool for investigating the behavior of the Lorentz channel only if W is sufficiently small. Indeed, only in such a case the dynamics of the Lorentz particles resembles that of the correlated random walker. In fact, if one considered the opposite limit, $W \to \infty$, a approaches 1, so that Eqs. (7) and (18) evaluate to $\alpha = 4/3$, $A = 1$, and $\beta = 0$, in contradiction with the expected $\alpha \leq 1$. In this limit the assumption about an invariant entry-exit trap velocity distribution breaks completely down. For the case of an uncorrelated random walk, characterized by $a = 1/2$, the equations would result in $A = (1 + n_x)^{-1}$ and $\beta = 1$, which are the proper expressions known for the Gambler's ruin model, but the Lorentz channel would then require a trap crossing probability of $\alpha = 1$, which is only realized in a cell without any obstacles. We mention these cases, that are not addressed in the present work, to highlight the fact that using a CRW as opposed to a random walk was essential in deriving fully consistent $A(W, n_x)$, and thus $\beta(W)$. For the characteristic W values one has $\beta(W_*) \approx 17/5 \approx 3.4 > 3$ and $\beta(W_c) \approx 7/3 \approx 2.33 < 3$, so that β exhibits a maximum with respect to W.

By exploiting the analogy with the CRW we have hence achieved a two-fold result: (i) Eq. (17) suggests that the effects on the transport properties of the Lorentz channel of the geometry of the elementary cell and of the number of elementary cells are factorized. In particular, for all values of W, the ratio of the reflected to the transmitted fluxes depends linearly on n_x with a proportionality coefficient that encodes the effects of the geometry of the elementary cell composed of identical, but non-aligned traps. (ii) The geometry of the cell enters in Eq. (18) through the cell crossing probability a. For the Lorentz channel it is in turn determined by the trap crossing probability $\alpha(W)$. Other arrangements of traps in a modified cell would lead to different expressions for a in terms of α, while α remains unaffected.

The result of the numerical computation is reported in Fig. 6 where a is represented by the red line. The probability a has been computed not only in the region of interest, namely $W \in (0, W_c]$, but also for larger values of W to check the consistency of our results. As expected, a tends to 1 when W tends to infinity, indeed, when the scatterers are small the probability to cross the elementary cell grows. For W small α tends to 2/3, a tends to 1/4, and A tends to $(1 + 3n_x)^{-1} < 1/4$. It is remarkable that for small values of W, approximately from 0 to 1/20, a is a decreasing, rather than increasing function of W. In Appendix D, we give an explanation for this fact.

5. Diffusion coefficient

Using the CRW approach, we have access to various additional quantities that characterize the channel such as the mean square displacement (MSD) of particle positions, as well as the diffusion coefficient D_x. The diffusion coefficient D of the infinite lattice of traps had been studied by Machta and Zwanzig [8] and follow-up works [10,13,31]. Furthermore, properties of the diffusion coefficient in correlated random walks on various types of lattices have been explored in [32,33], whereas applications to a three-dimensional periodic Lorentz gas have been treated in [34]. For our system, the x-component of the diffusion coefficient can be measured from particle trajectories in the infinite channel via the velocity autocorrelation function $D_x = \int_0^\infty \langle v_x(t)v_x(0)\rangle\, dt$, or equivalently, exploiting the one-dimensional CRW, via the asymptotic MSD

$$D_x = \lim_{t\to\infty} \frac{\langle [x(t) - x(0)]^2\rangle}{2t}, \tag{20}$$

where the brackets denote an average over an ensemble of realizations of the CRW, originating from different initial data for the particle position and velocity. The CRW can be regarded as representing the motion of a walker traveling at constant speed $v_{\rm cell} = \sqrt{3}h/\tau_{\rm cell}$ from cell (or column) to adjacent cell (or column) within a certain time interval $\tau_{\rm cell}$. The initial position and velocity of the walker are denoted by $x(0) = x_0$ and $v_x(0) = v_0 = \pm v_{\rm cell}$. At the kth transit between cells the walker's velocity is recursively determined by

$$v_k = \begin{cases} +v_{k-1}, & \text{probability } a, \\ -v_{k-1}, & \text{probability } 1-a. \end{cases} \tag{21}$$

At the kth transit the walker is hence at position x_k of a vertical gate separating cells, given by

$$x_k = x_{k-1} + v_{k-1}\tau_{\rm cell} = x_0 + \tau_{\rm cell}\sum_{j=0}^{k-1} v_j, \tag{22}$$

and thus

$$\frac{\langle (x_k - x_0)^2\rangle}{\tau_{\rm cell}^2} = \sum_{i=0}^{k-1}\sum_{j=0}^{k-1}\langle v_i v_j\rangle. \tag{23}$$

To compute the velocity truncated autocorrelation required in Eq. (23), we just have to notice that the sign of the velocity is flipped with probability a, so that, for $s > 0$,

$$\langle v_k v_{k\pm s}\rangle = \sum_{r=0}^{s-1}\binom{s-1}{r} a^r(1-a)^{s-1-r}(-1)^{s-1-r}v_k^2$$

and, hence,

$$\begin{aligned}\langle v_k v_{k\pm s}\rangle &= v_{\rm cell}^2\sum_{r=0}^{s-1}\binom{s-1}{r} a^r(a-1)^{s-1-r} \\ &= v_{\rm cell}^2(2a-1)^s. \end{aligned}\tag{24}$$

Now, from (23) and (24) it follows that

$$\frac{\langle (x_k - x_0)^2\rangle}{(\tau_{\rm cell}v_{\rm cell})^2} = \sum_{i=0}^{k-1}\sum_{s=-i}^{k-1-i}(2a-1)^{|s|}, \tag{25}$$

and, thus, the MSD at the kth transit becomes

$$\begin{aligned}\frac{\langle (x_k - x_0)^2\rangle}{3h^2} &= \sum_{i=0}^{k-1}\left[-1 + \frac{1-(2a-1)^{i+1}}{1-(2a-1)} + \frac{1-(2a-1)^{k-i}}{1-(2a-1)}\right] \\ &= \left[\frac{a}{1-a} - \frac{2a-1-(2a-1)^{1+k}}{2k(1-a)^2}\right]k. \end{aligned}\tag{26}$$

where we made use of $v_{\rm cell}\tau_{\rm cell} = \sqrt{3}h$. The MSD (and its derivative with respect to k) monotonically increase with increasing k only for $a \geq 1/4$ (and $a \geq 1/2$). Within the regime $a < 1/4$, which we observe for $W \leq W_{\rm cf}$ (Fig. 6), the MSD (26) therefore oscillates with k.

Since the 2nd term in the bracket tends to zero for $k \to \infty$, the diffusion coefficient obtained from the MSD is

$$D_x = \lim_{k\to\infty}\frac{\langle (x_k - x_0)^2\rangle}{2k\tau_{\rm cell}} = \frac{a}{2(1-a)}\frac{3h^2}{\tau_{\rm cell}}. \tag{27}$$

These are exact result for the MSD and diffusion coefficient of the CRW. They reduce to the familiar random walk results for $a = 1/2$, i.e., for equal forward–backward probabilities in Eq. (21). Using a in terms of α or β, we finally obtain from Eq. (27)

$$D_x = \frac{1}{2\beta}\frac{3h^2}{\tau_{\rm cell}} = \frac{\alpha}{2(4-3\alpha)}\frac{3h^2}{\tau_{\rm cell}}. \tag{28}$$

The same replacement can be done in the expression (26) for the MSD. Using $\tau_{\rm cell}$ and $\tau_{\rm trap}$ from Eqs. (A.1) and (3), as well as the definition of W, one arrives at the following result:

$$D_x = \frac{3\alpha}{(4-3\alpha)}\,\frac{W(W+2)^2}{\pi[\sqrt{3}(W+2)^2 - 2\pi]}sv, \tag{29}$$

where s is the radius of the scatterers and v the speed of the moving particles. Because $\alpha \to 2/3$ for $W \to 0$, the prefactor $3\alpha/(4-3\alpha)$ tends to one, thus recovering the random walk result derived through a different approach in [8]. For $\alpha(W_*) \approx 5/8$ and $\alpha(W_c) \approx 3/4$, the prefactor evaluates to $15/17 < 1$ and $9/7 > 1$, respectively. This non-monotonic behavior of the prefactor correctly captures the departure between measured and earlier predicted D_x (Fig. 11). We obtained the value of $D_x(W_c) \approx (0.230 \pm 0.002)sv$ using the velocity autocorrelation function (20). The same had been reported before using various methods [13]. Our Eq. (29) predicts $D_x(W_c) \approx 0.228583\, sv$, in agreement with the measurement, while the existing approaches resulted in $D_x(W_c) \approx 0.178\, sv$ [8], $D_x(W_c) \approx 0.20\, sv$ using a prefactor $3\alpha/2$ [13] in the above analytic expression (29), $D_x(W_c) \approx 0.26\, sv$ using a 3rd order numerical approximation [13], and $D_x(W_c) \approx 0.25\, sv$ using the Boltzmann approximation, useful only at $W \approx W_c$, supplemented by an arbitrary shift $\Delta D_x = 0.025\, sv$ [13] to best capture the known result. In short, we have demonstrated here that it is important to use the CRW approach to derive D_x with the proper prefactor.

Analytic expressions capturing D_x and α in terms of W alone are available in Appendix C. We also note in passing that the calculation of the MSD presented here proceeds analogous to the calculation of the mean squared end-to-end distance of a freely rotating or wormlike (macromolecular) chain with fixed bending angle $\vartheta = \cos^{-1}(2a-1)$ and k bonds [35]. The leading $a/(1-a) = (1+\cos\vartheta)/(1-\cos\vartheta)$ term in Eq. (26) is known as Flory's characteristic ratio in chemistry, and the persistence length L_p of the walk, usually defined by $\langle v_k v_{k\pm s}\rangle \propto e^{-s/L_p}$, remains undefined as $2a < 1$ in our case. The most common chain models are CRWs [35–38].

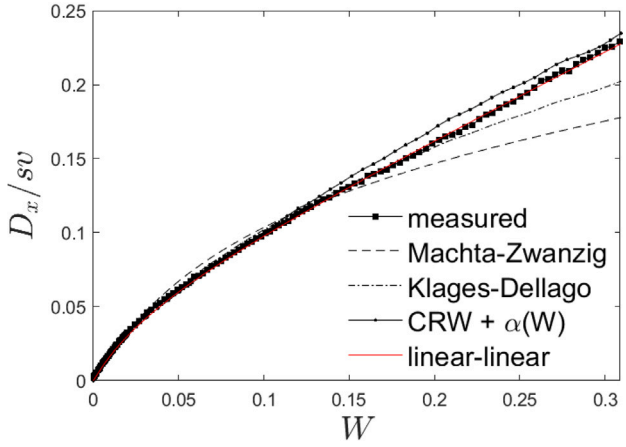

Fig. 11. Diffusion coefficient D_x measured via the velocity autocorrelation function (20), compared with the Machta-Zwanzig result [8], the Klages-Dellago result [13], and the results obtained here (CRW with the measured $\alpha(W)$ (29) and linear–linear form (C.1)). While Machta-Zwanzig used Eq. (29) with prefactor unity, Klages-Dellago derived Eq. (29) with prefactor $3\alpha/2$. Our prefactor derived using the CRW removes the overshoot at $W \approx W_*$ and matches $D(W_c)$, while it slightly overestimated D at $W \approx 0.2$.

6. Conclusions

This paper focused on the role of finite size effects in the analysis of the transmission coefficient for a 2D Lorentz gas model. We have considered a finite rectangular Lorentz channel, consisting of point particles moving in an environment made of regularly placed hard disks. Particles enter from the left boundary and exit from both left and right boundaries, which are separated by n_x elementary cells. The top and bottom sides of the channel are implemented as periodic boundary conditions, which are equivalent to reflecting boundaries, as far as transport properties are concerned. We only consider the cases of finite horizon, $W \leq W_c$, that asymptotically enjoy normal diffusion, as proven following the dynamics from collision to collision, under the coarse-graining associated with a scaling in which time grows without bounds and coordinates are divided by the square root of time [7]. In these cases, a finite diffusion coefficient exists because the particles MSD grows asymptotically linearly with time t, see Section 5 for the associated CRW. In the infinite horizon case, $W > W_c$, diffusion turns anomalous: the diffusion coefficient does not exist because a logarithmic correction is added to the growth in time of the MSD, which asymptotically goes like $t \ln t$ [15,16]. Therefore, the statistic turns problematic and several our assumptions, that are accurately verified in the finite horizon cases, break down.

Within the finite horizon case, there is a perfect match between the statistic of the dynamics of the Lorentz channel and the exact calculations based on a suitable CRW. In fact, we obtained analytic expressions for all quantities in terms of W and n_x, with no free parameters left. These expressions are more and more accurate as W is decreased, or n_x is increased. In fact, the effectiveness of the stochastic descriptions we have adopted derives from the decay of correlations, and this feature of dispersive billiards derives from collisions, which are more numerous within our channels if W decreases or n_x increases. Therefore, at given W and n_x, using the numerically obtained values of $\alpha(W)$, instead of the corresponding analytic approximations, improves the accuracy of the analytic expressions for the remaining quantities considered here.

Our calculations prove that Machta and Zwanzig's phase-space and area arguments towards the calculation of τ_{trap} can be extended to cells and channels. With the caveat, that they increasingly fail with increasing imbalance between crossing and backscattering times in the unit cells.

We found an analytical expression for $(1 - A)/A$, with A the probability that a particle entering the channel from one side exits through the opposing side. This quantity results proportional to n_x. The proportionality factor $\beta(W)$ depends on the size of the system, and correctly represents the finite size effects, due to the finite value of n_x, (Fig. 3-b). The agreement of the analytical expressions derived from the CRW, and the numerical results obtained from direct simulations of the deterministic particle dynamics, unambiguously quantify the scales of interest. The one of the microscopic dynamics is given by the free flights from collision to collision, or by the size of the traps, in the billiard table, and is represented by the CRW process with preferred back scattering. The mesoscopic scale is of the order of a limited number of elementary cells, in the billiard table, and is equivalent to a Markov process. Finally, the macroscopic scale is achieved when the number of cells n_x is large, and normal diffusion takes place in the bulk of the channel, located far away from the left and right boundaries. The corresponding stochastic counterpart, in this case, is that of a Wiener process that amounts to diffusion on a proper coarse-grained scale, see also Appendix E for a related discussion. Our work explicitly quantifies the corrections due to the finite size of the channel (Section 5).

Application of the theory developed in this work will be considered in future works. They concern the linear transport phenomena, and their corrections in the case of the small systems of interest in bio- and nano-technologies. Also non-equilibrium phase transitions, occurring in systems such as those of Refs. [39–43], will be addressed.

CRediT authorship contribution statement

Emilio N.M. Cirillo: Writing – review & editing, Validation, Methodology, Investigation, Conceptualization. **Matteo Colangeli:** Writing – review & editing, Writing – original draft, Project administration, Methodology, Investigation, Formal analysis, Conceptualization. **Martin Kröger:** Writing – review & editing, Writing – original draft, Visualization, Software, Methodology, Investigation, Formal analysis. **Lamberto Rondoni:** Writing – review & editing, Supervision, Methodology, Formal analysis, Conceptualization.

Declaration of competing interest

The authors declare that they have no known competing financial interests or personal relationships that could have appeared to influence the work reported in this paper.

Acknowledgments

The authors gratefully acknowledge valuable discussions with H. Van Beijeren. This work was carried out under the auspices of the Italian National Group of Mathematical Physics. LR gratefully acknowledges support from the Italian Ministry of University and Research (MUR) through the grant PRIN2022-PNRR project (No. P2022Z7ZAJ) "A Unitary Mathematical Framework for Modelling Muscular Dystrophies" (CUP: E53D2301807 0001). ENMC and MC thank the PRIN 2022 project "Mathematical Modelling of Heterogeneous Systems (MMHS)", financed by the European Union - Next Generation EU, CUP B53D 23009360006, Project Code 2022MKB7MM, PNRR M4.C2.1.1.

Appendix A. Cell residence times

Extending Machta and Zwanzig's approach [8] for traps to our setup made of cells, the total volume of phase space associated with a single column of cells is determined by the fraction of phase space available for exiting a cell in horizontal direction. This fraction is insensitive to n_y. The total volume of phase space associated with a single cell is $2\pi A_{\text{cell}}$, where $A_{\text{cell}} = \sqrt{3}h^2 - 2\pi s^2$ is the void area of a single cell. The factor 2π is the measure of velocity space. The portion of this phase space from which a walker escapes from a column in a time less than

δt has a volume $2(h-2s)\delta t \int_0^\pi v \sin\theta \, d\theta = 4(h-2s)v\delta t$ since $2(h-2s)$ is the total length of the two exits of a cell. The average time spent in a column is therefore estimated to be

$$\tau_{\text{cell}} = \frac{\pi A_{\text{cell}}}{2(h-2s)v} = 6\tau_{\text{trap}}, \tag{A.1}$$

where we have expressed τ_{trap} in terms of W earlier, c.f., Eq. (3). This expression reduces to $\tau_{\text{cell}} = (\pi/2)\sqrt{3}h/v$ for $s = 0$, in agreement with our earlier 2D result for empty passive channels, namely $\tau_p = n_x \tau_{\text{cell}} = (\pi/2)\ell_p/v$ with channel length $\ell_p = n_x\sqrt{3}h$.

In the first part of this appendix we are going to show how the result (A.1) can be reproduced using the transition matrix $\mathbf{Q}$ defined by Eq. (6) for a single cell, upon making the assumption that the crossing and backscatter times in a trap, here denoted by $\tau^{\hookrightarrow}_{\text{trap}}$ and $\tau^{\hookleftarrow}_{\text{trap}}$, are identical. The derivation provides additional information to be used in the 2nd part of this appendix, where we release this assumption.

We begin with the first part. Using the transition matrix $\mathbf{Q}$ in terms of the trap crossing probability α, the probability a_t that a particle passes the cell after visiting t traps is

$$a_t = (\mathbf{Q}^{t-1})_{17} Q_{78}. \tag{A.2}$$

Similarly, the probability b_t that a particle returns to the previous cell after visiting t traps is

$$b_t = \delta_{t,1} Q_{10} + \left(\mathbf{Q}^{t-1}\right)_{12} Q_{20}. \tag{A.3}$$

Obviously, $a_t + b_t \neq 0$ and the cell crossing probability evaluates to $a = \sum_{t=1}^{\infty} a_t = 1 - \sum_{t=1}^{\infty} b_t = N_{17}Q_{78}$, where $\mathbf{N} = (\mathbb{I} - \mathbf{Q})^{-1}$, in agreement with Eq. (7). We are interested in τ_{cell}, the average time a particle spends in a cell. The residence time is different for particles that pass, compared with particles that backscatter, so lets first calculate the conditional counterparts separately and denote them by $\tau^{\hookrightarrow}_{\text{cell}}$ and $\tau^{\hookleftarrow}_{\text{cell}}$, respectively, and lateron obtain τ_{cell}. One has, using the definitions of a_t and b_t, and for the time being making the incorrect assumption that mean crossing $\tau^{\hookrightarrow}_{\text{trap}}$ and mean backscatter $\tau^{\hookleftarrow}_{\text{trap}}$ times in a trap are identical, and both identical with τ_{trap},

$$\frac{\tau^{\hookrightarrow}_{\text{cell}}}{\tau_{\text{trap}}} = \frac{1}{a}\sum_{t=1}^{\infty} t a_t, \qquad \frac{\tau^{\hookleftarrow}_{\text{cell}}}{\tau_{\text{trap}}} = \frac{1}{1-a}\sum_{t=1}^{\infty} t b_t, \tag{A.4}$$

and thus

$$\tau_{\text{cell}} = a\tau^{\hookrightarrow}_{\text{cell}} + (1-a)\tau^{\hookleftarrow}_{\text{cell}} = \left[\sum_{t=1}^{\infty} t a_t + \sum_{t=1}^{\infty} t b_t\right] \tau_{\text{trap}}. \tag{A.5}$$

The sums can be evaluated exactly using basic properties of the geometric series for matrices,

$$\sum_{t=1}^{\infty} t a_t = (\mathbf{N}^2)_{17} Q_{78} = \frac{(\mathbf{N}^2)_{17}}{N_{17}} a = \frac{(8-3\alpha)^2}{8(2-\alpha)^2}, \tag{A.6}$$

$$\sum_{t=1}^{\infty} t b_t = Q_{10} + (\mathbf{N}^2)_{12} Q_{20} = \frac{128 - 3\alpha(48-13\alpha)}{8(2-\alpha)^2}. \tag{A.7}$$

Inserting Eq. (A.6) and (A.7) into Eq. (A.4) yields

$$\frac{\tau^{\hookrightarrow}_{\text{cell}}}{\tau_{\text{trap}}} = \frac{1}{2(2-\alpha)} + \frac{8}{\alpha} - \frac{9}{4}, \tag{A.8}$$

$$\frac{\tau^{\hookleftarrow}_{\text{cell}}}{\tau_{\text{trap}}} = \frac{1}{2(2-\alpha)} + \frac{2}{4-3\alpha} + \frac{13}{4}, \tag{A.9}$$

and thus finally, upon inserting Eqs. (A.8)–(A.9) into Eq. (A.5), we recover Machta and Zwanzig's estimate (A.1). This calculation, based on the assumption $\tau^{\hookrightarrow}_{\text{trap}} = \tau^{\hookleftarrow}_{\text{trap}} = \tau_{\text{trap}}$, gets more and more accurate as W tends to 0. This statement completes the first part of this appendix.

In the following 2nd part, we release this assumption and proceed with the exact calculation of the unconditional and conditional mean cell residence times τ_{cell}, $\tau^{\hookrightarrow}_{\text{cell}}$, and $\tau^{\hookleftarrow}_{\text{cell}}$. One way to do this analytically is to replace $\mathbf{Q}$ by a matrix $\tilde{\mathbf{Q}}$ that still contains information about forward and backward, so that $\tilde{\mathbf{Q}}^{t-1}$ provides the whole distribution of accumulated mean times that passed during t visits. Because an exponential function has the necessary feature that multiplication is equivalent with addition of its arguments, one can encode the information about forward and backward using an exponential, $\tilde{Q}_{ji} = Q_{ji}\exp(\lambda\tau^{\hookrightarrow}_{\text{trap}})$ for all forward terms (left hand side of Eq. (6)), and $\tilde{Q}_{ji} = Q_{ji}\exp(\lambda\tau^{\hookleftarrow}_{\text{trap}})$ for all remaining backward terms, where we introduced λ just to be able to project out the argument of the exponential via a derivative with respect to λ. To summarize, and to be more specific, using the modified $\tilde{a}_t(\lambda) = (\tilde{\mathbf{Q}}^{t-1})_{17}\tilde{Q}_{78}$, and with the cumulant-generating function $G_a(\lambda) = \ln\sum_{t=1}^{\infty}\tilde{a}_t(\lambda)$, and $\tilde{\mathbf{N}}(\lambda) = (\mathbb{I} - \tilde{\mathbf{Q}})^{-1}$, one has

$$\begin{aligned}
\tau^{\hookrightarrow}_{\text{cell}} &= G_a'(0) \\
&= \frac{d}{d\lambda}\ln\sum_{t=1}^{\infty}\tilde{a}_t\bigg|_{\lambda=0} \\
&= \frac{\left[(d/d\lambda)\sum_{t=1}^{\infty}(\tilde{\mathbf{Q}}^{t-1})_{17}\tilde{Q}_{78}\right]_{\lambda=0}}{\sum_{t=1}^{\infty} a_t} \\
&= \frac{\left[(d/d\lambda)(\mathbb{I}-\tilde{\mathbf{Q}})^{-1}_{17}\tilde{Q}_{78}\right]_{\lambda=0}}{N_{17}Q_{78}} \\
&= \frac{\left[\tilde{N}_{17}\tilde{Q}'_{78} + \tilde{N}'_{17}\tilde{Q}_{78}\right]_{\lambda=0}}{a} \\
&= \frac{\tau^{\hookrightarrow}_{\text{trap}} N_{17}Q_{78} + \tilde{N}'_{17}(0)Q_{78}}{a} \\
&= \tau^{\hookrightarrow}_{\text{trap}} + \frac{\tilde{N}'_{17}(0)\alpha}{2a} \\
&= \frac{12a(1+a)\tau^{\hookrightarrow}_{\text{trap}} + (4+2a^3-3a^2)\tau^{\hookleftarrow}_{\text{trap}}}{2a(1+2a)},
\end{aligned} \tag{A.10}$$

where the prime denotes a derivative with respect to λ. Above, we added some intermediate steps for easier comparison with the following Appendix B. This expression (A.10) properly reduces to (A.8) for $\tau^{\hookleftarrow}_{\text{trap}} = \tau^{\hookrightarrow}_{\text{trap}}$. Higher moments, such as the mean squared crossing time are contained in $G_a(\lambda)$ as well.

In a completely analogous fashion, with $G_b(\lambda) = \ln\sum_{t=1}^{\infty}\tilde{b}_t(\lambda)$ one obtains

$$\begin{aligned}
\tau^{\hookleftarrow}_{\text{cell}} &= G_b'(0) \\
&= \frac{[\tilde{Q}'_{10} + \tilde{N}'_{12}\tilde{Q}_{20} + \tilde{N}_{12}\tilde{Q}'_{20}]_{\lambda=0}}{1-a} \\
&= \frac{4a(5-3a)\tau^{\hookrightarrow}_{\text{trap}} + (8-8a+3a^2-2a^3)\tau^{\hookleftarrow}_{\text{trap}}}{2(1-a)(1+2a)}.
\end{aligned} \tag{A.11}$$

It is worth noticing that $\tau^{\hookrightarrow}_{\text{cell}}$ and $\tau^{\hookleftarrow}_{\text{cell}}$, as opposed to $\tau^{\hookrightarrow}_{\text{trap}}$ and $\tau^{\hookleftarrow}_{\text{trap}}$ (Fig. 8), are very different not only in magnitude but also in their dependency with respect to a, α, and thus W. While $\tau^{\hookrightarrow}_{\text{cell}}$ monotonically decreases with increasing α, $\tau^{\hookleftarrow}_{\text{cell}}$ increases, but stays well below $\tau^{\hookrightarrow}_{\text{cell}}$ for any possible α. In the limit of small $W \ll W_c$, $\tau^{\hookrightarrow}_{\text{cell}}/\tau_{\text{trap}}$ approaches $81/8 \approx 10.1$, while $\tau^{\hookleftarrow}_{\text{cell}}/\tau_{\text{trap}}$ approaches $37/8 \approx 4.6$.

With expressions (A.10) and (A.11) at hand, the mean cell residence time becomes

$$\begin{aligned}
\tau_{\text{cell}} &= a\tau^{\hookrightarrow}_{\text{cell}} + (1-a)\tau^{\hookleftarrow}_{\text{cell}} \\
&= 4\alpha\tau^{\hookrightarrow}_{\text{trap}} + (6-4\alpha)\tau^{\hookleftarrow}_{\text{trap}}.
\end{aligned} \tag{A.12}$$

The here derived final results for $\tau^{\hookrightarrow}_{\text{cell}}$, $\tau^{\hookleftarrow}_{\text{cell}}$, and τ_{cell} cannot be estimated using Machta and Zwanzig's approach, that however remains useful as long as $\tau^{\hookrightarrow}_{\text{trap}}$ and $\tau^{\hookleftarrow}_{\text{trap}}$ are very similar. But they can alternatively be obtained from the perspective of the fundamental matrix $\mathbf{N}$, instead of making use of a_t, b_t and a cumulant-generating function (sometimes also denoted as partition sum, as we implicitly introduced a hamiltonian). Since calculating the conditional and unconditional residence times in the channel requires repeating the calculations using a different Markov chain and thus a different $\mathbf{Q}$, we are going to introduce this alternative language in the following Appendix B. Since $\tau^{\hookrightarrow}_{\text{cell}}$ and $\tau^{\hookleftarrow}_{\text{cell}}$ were shown to be very different, it will be important to not assume that they are equal.

Higher cumulants of the distributions of unconditional and conditional cell residence times can be calculated along the lines indicated in the present appendix. The full distributions are shown in Fig. 12.

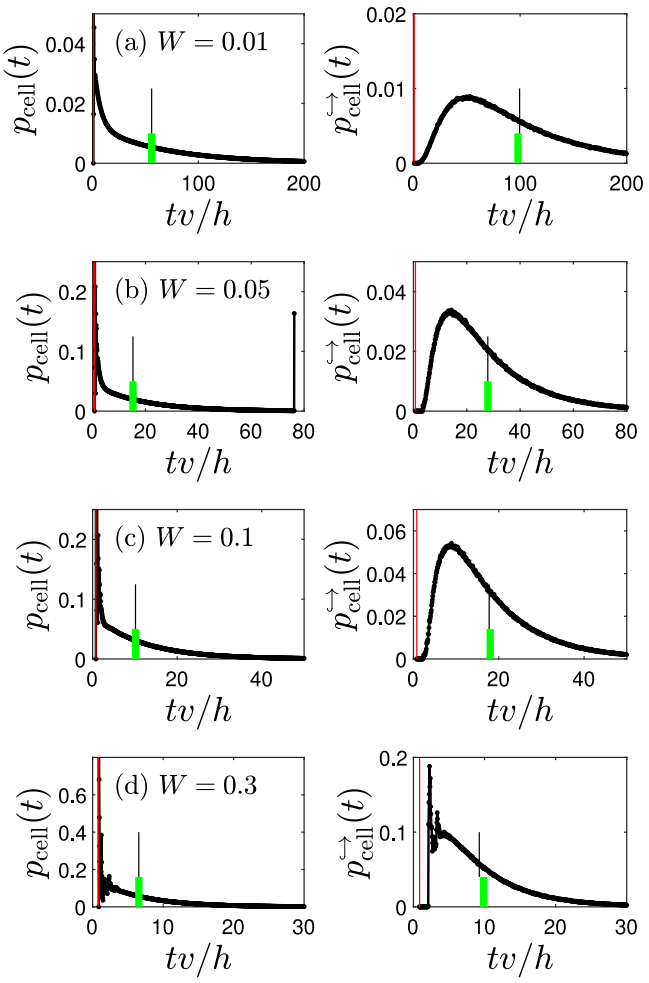

Fig. 12. Single cell at (a) $W = 0.01$, (b) 0.05, (c) 0.1, and (d) 0.3. The left column refers to the cell residence (unconditioned) time distribution $p_{\rm cell}(t)$, the right column to the mean crossing time distribution $p^{\hookrightarrow}_{\rm cell}(t)$ (black squares, measured). The red vertical line marks $t = [\sqrt{3} - 2(2+W)^{-1}]h/v$. The green vertical line marks the analytical result for the mean residence $\tau_{\rm cell}$ and mean crossing time $\tau^{\hookrightarrow}_{\rm cell}$, assuming $\tau^{\hookrightarrow}_{\rm trap} = \tau^{\leftrightarrow}_{\rm trap} = \tau_{\rm trap}$, according to Eqs. (3), (A.12), (A.10), (C.2), while the vertical black line marks the measured mean residence and mean crossing times for comparison with the analytical result. Distributions obtained using 10^7 independent realizations.

Appendix B. Channel residence times

Extending Machta and Zwanzig's approach [8] for traps to a channel, and for a moment assuming the incorrect $\tau^{\hookrightarrow}_{\rm cell} = \tau^{\leftrightarrow}_{\rm cell}$ to hold, the average time spent in a channel is

$$\tau_{\rm channel} = n_x \tau_{\rm cell} = 6 n_x \tau_{\rm trap}, \tag{B.1}$$

so that we know via Eq. (3) the residence times in traps, cells, and channel analytically in terms of all system variables, including W. Such expressions are not only useful as they enter the diffusion coefficient, but we use them to estimate the minimum duration of simulation runs. The mean number of collisions is then also known analytically for cells and channels. For a channel, the mean number of collisions, before a particle exits the channel, is $c_{\rm channel} = 2\pi n_x/W$, in particular. We know from the preceding section, that $\tau^{\hookrightarrow}_{\rm cell} \neq \tau^{\leftrightarrow}_{\rm cell}$.

Here we are therefore interested in calculating the mean residence time in the channel as well as the mean crossing time through the channel. While the former, denoted as $\tau_{\rm channel}$, is the typical time spent in the channel by a particle entered through the left side before exiting through *either* of the two sides, the latter, denoted as $\tau^{\hookrightarrow}_{\rm channel}$, corresponds to the typical time taken by a particle, that entered through the left side of the channel, to exit through the opposite side. To estimate the two quantities we adapt the approach used for a cell in Appendix A.

We hence consider an absorbing Markov chain on a state space defined as follows. We associate the index $2k-1$, with $k = 1, \dots, n_x$, to the state $(k, +1)$, corresponding to a particle located in the kth cell of the channel and equipped with a positive velocity (i.e. pointing rightward). Analogously, we associate the index $2k$ to the state $(k, -1)$, corresponding to a particle residing in the kth cell and equipped with a negative velocity. Therefore, $\Lambda = \{1, 2, \dots, 2n_x - 1, 2n_x\}$ identifies the set of transient states of the chain, with 0 and $2n_x + 1$ corresponding to the absorbing states. We then introduce a $2n_x \times 2n_x$ transition matrix $\mathbf{Q}$, whose components Q_{ji}, with $j, i \in \Lambda$, read

$$Q_{ji} = \begin{cases} a, & i = j+2, \text{odd } j \\ 1-a, & i = j+1, \text{even } j \\ 1-a, & i = j-1, \text{odd } j \\ a, & i = j-2, \text{even } j \\ 0, & \text{otherwise,} \end{cases} \tag{B.2}$$

where a is our cell crossing probability. Following the approach worked out in Appendix A, both $\tau^{\hookrightarrow}_{\rm channel}$ and $\tau^{\leftrightarrow}_{\rm channel}$ are obtained from the modified $\tilde{\mathbf{Q}}(\lambda)$, which is obtained from $\mathbf{Q}$ upon replacing a in the forward terms by $a\exp(\lambda\tau^{\hookrightarrow}_{\rm cell})$ and $(1-a)$ in the backward terms by $(1-a)\exp(\lambda\tau^{\leftrightarrow}_{\rm cell})$. With this new $2n_x \times 2n_x$ matrix at hand, $\tilde{\mathbf{N}}(\lambda) = (\mathbb{I} - \tilde{\mathbf{Q}})^{-1}$, and

$$\tau^{\hookrightarrow}_{\rm channel} = \tau^{\hookrightarrow}_{\rm cell} + \frac{\tilde{N}'_{1,2n_x-1}(0)}{\tilde{N}_{1,2n_x-1}(0)}, \tag{B.3}$$

$$\tau^{\leftrightarrow}_{\rm channel} = \frac{[\tilde{Q}'_{10} + \tilde{N}'_{12}\tilde{Q}_{20} + \tilde{N}_{12}\tilde{Q}'_{20}]_{\lambda=0}}{\tilde{Q}_{10}(0) + \tilde{Q}_{20}(0)\tilde{N}_{1,2}(0)}, \tag{B.4}$$

in a full analogy with Eqs. (A.10) and (A.11) for the 9 states model of a cell. Accordingly, here we have to use $\tilde{Q}_{10} = (1-a)\exp(\lambda\tau^{\leftrightarrow}_{\rm cell})$ and $\tilde{Q}_{20} = a\exp(\lambda\tau^{\hookrightarrow}_{\rm cell})$. As before, the prime denotes a derivative with respect to λ. Note that the channel pass probability A, calculated using the CRW approach in Eq. (14), is recovered via $A = a\tilde{N}_{1,2n_x-1}(0)$.

The expressions (B.3) and (B.4) can be worked out conveniently using various methods. Using any of them, one arrives at

$$\begin{aligned} \tau^{\hookrightarrow}_{\rm channel} &= \frac{[1 + b + 2a^2 + b(3a + bn_x)n_x]n_x}{3(a + bn_x)}\tau^{\hookrightarrow}_{\rm cell} \\ &\quad + \frac{b^2(1 + bn_x + 2a)(n_x - 1)n_x}{3a(a + bn_x)}\tau^{\leftrightarrow}_{\rm cell}, \end{aligned} \tag{B.5}$$

$$\begin{aligned} \tau^{\leftrightarrow}_{\rm channel} &= \frac{a(a + 2 + 2bn_x)(n_x - 1)}{3(a + bn_x)}\tau^{\hookrightarrow}_{\rm cell} \\ &\quad + \frac{1}{3}\left[a + 2bn_x + \frac{1+a}{a + bn_x}\right]\tau^{\leftrightarrow}_{\rm cell}, \end{aligned} \tag{B.6}$$

where we used $b = 1 - a$ to shorten the expression. We successfully validated expressions (B.5) and (B.6) against the numerical implementation of the underlying Markov chain. Inline with the definitions of the conditional residence times, the mean channel residence time is given by $\tau_{\rm channel} = A\tau^{\hookrightarrow}_{\rm channel} + (1-A)\tau^{\leftrightarrow}_{\rm channel}$ with A from Eq. (14).

The resulting expressions for the mean crossing time in the channel are relevant as they provide a lower limit of the simulation time required to evaluate averages. Note that $\tau^{\hookrightarrow}_{\rm channel}$ is much larger than $\tau^{\leftrightarrow}_{\rm channel}$ for any n_x and that their ratio linearly increases with n_x,

$$\lim_{n_x \to \infty} \frac{\tau^{\hookrightarrow}_{\rm channel}}{n_x \tau^{\leftrightarrow}_{\rm channel}} = \frac{1-a}{2a}. \tag{B.7}$$

In the limit $W \to 0$, where α approaches $2/3$ and $\tau_{\rm trap}W$ approaches $(2\sqrt{3} - \pi)\pi s/6v$, as derived in the main text, while $s/6v$ is the mean time between collisions, the dimensionless times $\tau^{\hookrightarrow}_{\rm channel}$ and $\tau^{\leftrightarrow}_{\rm channel}$, multiplied by W, approach the values

$$\begin{aligned} \lim_{W \to 0} \frac{\tau^{\hookrightarrow}_{\rm channel} vW}{c_0 s} &= \frac{[3(1+n_x)n_x - 2]n_x}{1 + 3n_x}, \\ \lim_{W \to 0} \frac{\tau^{\leftrightarrow}_{\rm channel} vW}{c_0 s} &= \frac{1 + n_x + 2n_x^2}{1 + 3n_x}. \end{aligned} \tag{B.8}$$

where $c_0 = (2\sqrt{3} - \pi)\pi \approx 1.013$.

With this we have derived analytic expressions for mean channel residence, crossing and backscattering times, in terms of W, n_x, s, and v, valid for $W \ll W_c$. We confirmed that Machta and Zwanzig's estimate for the residence time is exact provided $\tau^{\hookrightarrow}_{\text{cell}} = \tau^{\hookleftarrow}_{\text{cell}}$. This equality does not hold in the present context. We use the mean crossing time in a channel (B.5) to estimate a lower limit for the computational effort (proportional to the number of collisions) in studying the 2D Lorentz channel at given n_x.

Appendix C. Analytic expression capturing the measured D_x

Since D_x is linear in W at small $W \ll W_c$ and in the vicinity of $W = W_c$, the simple "linear-linear" form

$$D_x = c_1 \frac{W(1 + 4\pi W/\sqrt{3})}{1 + c_2 W} sv \tag{C.1}$$

serves to excellently (Fig. 11) capture the measured D_x, while the two coefficients c_1 and c_2 are fully determined by $\alpha(0) = 2/3$ and $\alpha(W_c) = 3/4$, in light of Eq. (29). To be specific $c_1 = (\sqrt{3}\pi - \pi^2/2)^{-1} \approx 1.974$ and $c_2 \approx 25.8$. This implies

$$\alpha(W) \approx \frac{2}{3} \frac{1 + W[17.996 + W(80.614 + 19.482\,W)]}{1 + W[22.398 + W(53.332 + 12.967\,W)]}, \tag{C.2}$$

and similar parameter-free expressions for $a(W)$, $\beta(W)$, $\tau^{\hookrightarrow}_{\text{cell}}$, $\tau^{\hookleftarrow}_{\text{cell}}$, $\tau^{\hookrightarrow}_{\text{channel}}$, $\tau^{\hookleftarrow}_{\text{channel}}$, $\mathbf{Q}$, the MSD, $A(W, n_x)$ etc. While this expression (C.2) captures the measured α only qualitatively, the most important feature is that it exhibits a minimum at about $W \approx 0.046$. As obvious from the form of D_x in Eq. (C.1), it is a direct consequence of the relationship (29) combined with the different slopes of D_x at small $W \ll W_c$ (slope $c_1 sv \approx 1.974\, sv$) and $W \approx W_c$ (slope $\approx 0.573\, sv$).

Appendix D. Characteristic values W_* and W_{cf}

Let $\mathbf{r}$ denote a particle position inside a trap and $\mathbf{v}$ a velocity vector at this position. The time of next collision with a circle of radius $s = h/(2 + W)$, centered at $\mathbf{c}_j$ is the solution to $\mathbf{r} + t\mathbf{v} = \mathbf{c}_j + s\mathbf{u}$, with unit vector $\mathbf{u}$. These two equations for the components are readily solved for t and $\mathbf{u}$, as $\mathbf{u}$ can be expressed through a single polar angle. From the two formal solutions the one with the smaller t applies, as our particles have to stay inside the trap. We hence have an analytic expression for a collision point $\mathbf{P}_j = \mathbf{P}_j(\mathbf{x}, \mathbf{v})$ residing on the perimeter of circle j in terms of $\mathbf{x}$ and $\mathbf{v}$. During the collision $\mathbf{v}$ receives its new direction $(\mathbb{I} - 2\mathbf{nn}) \cdot \mathbf{v}$ with surface normal $\mathbf{n} = (\mathbf{P}_j - \mathbf{c}_j)/|\mathbf{P}_j - \mathbf{c}_j|$. The three circles 1,2,3 enclosing a trap are centered at coordinates $\mathbf{c}_1 = (0, h/2) = -\mathbf{c}_2$ and $\mathbf{c}_3 = (\sqrt{3}h/2, 0)$, if we choose the origin of the coordinate system accordingly.

There are two special values of W that we would like to calculate here: (i) the smallest W, denoted as W_{cf} (collision-free), for which a particle, starting at a gap (of size $g = h - 2s$), can exit through another gap without colliding with any circle and (ii) the smallest W, denoted by W_*, for which a particle, starting from gap, cannot reach one of the opposing gaps without colliding with all three circles. Since W_* determined this way will turn out being comparable with the measured W_*, we use the same symbol.

Case (i) is relatively simple to calculate as one has to consider only the extreme situation, where a particle enters and exits a trap where a gap meets a circle (Fig. 13). These two positions are given by $\mathbf{x}_0 = \mathbf{c}_2 + s(\mathbf{c}_1 - \mathbf{c}_2)/h = (0, -g/2)$ and $\mathbf{x}_1 = \mathbf{c}_3 + s(\mathbf{c}_1 - \mathbf{c}_3)/h$. For the extreme case we are interested in, the line connecting $\mathbf{x}_0$ and $\mathbf{x}_1$ should meet circle 1 at its midpoint, i.e., $|\mathbf{c}_1 - (\mathbf{x}_0 + \mathbf{x}_1)/2| = s$. This yields

$$W_{\text{cf}} = \frac{2\sqrt{3} - 3}{3} \approx 0.1547. \tag{D.1}$$

Case (ii) is more easily done numerically, using the analytic expression for $\mathbf{P}_1(\mathbf{x}, \mathbf{y})$ and $\mathbf{P}_3$. One needs to follow the trajectory starting as for (i) where a trap meets circle 1, and then consider alternating collisions

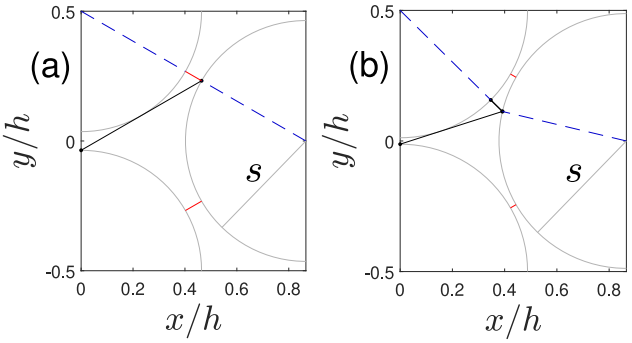

Fig. 13. Shown are special trap trajectories (solid black) of particles that enter a trap next to a circle for (a) $W = W_{\text{cf}} \approx 0.1547$ and (b) $W = W_* \approx 0.05$. The two situations are considered in Appendix D. Gaps separating traps have been added (red lines) to guide the eye. The three identical circles surrounding the trap have radius $s = h/(2 + W)$. While (a) shows the situation where a particle performs a collision-free flight inside a trap (for larger W, this is not possible anymore), (b) depicts the situation where the particle is backscattered to its original position after exactly three collisions plus two grazing contacts. The dashed blue lines have been added to see how calculate these two characteristic W values analytically. The polar angle of the initial velocity of the particle is determined by the condition of grazing contact.

with the two remaining circles 2 and 3. If W is too small, a particle cannot reach the gate between circles 2 and 3 by colliding with them, and gets returned into the interior of the trap, as the angle at which the particle enters the tubus in front of the gate is necessarily too large. As a result, the backscattering probability tends to increase with increasing W up to the W we are seeking for. For larger W the particles crossing probability increases with W, as the particle is usually not repelled by the region next to a trap. This purely geometric calculation boils down to calculating the W for which the situation in Fig. 13 applies. A particle entering at $\mathbf{x}_0 = (0, -g/2)$ with velocity $\mathbf{v}_0$, achieving grazing contact with circle 1, which determines $\mathbf{v}_0$ via $\mathbf{v}_0 \cdot \mathbf{c}_3/|\mathbf{c}_3| = s/(h - s)$, collides with the circle centered at $\mathbf{c}_3$ at collision point $\mathbf{x}_1 = \mathbf{P}_3(\mathbf{x}_0, \mathbf{v}_0)$, before being reflected in direction of the center $\mathbf{c}_1$. This latter condition translates into the equation $(\mathbf{c}_1 - \mathbf{x}_1)/|\mathbf{c}_1 - \mathbf{x}_1| = (\mathbf{I} - 2\mathbf{nn}) \cdot \mathbf{v}_0$ with collision normal $\mathbf{n} = (\mathbf{x}_1 - \mathbf{c}_3)/|\mathbf{x}_1 - \mathbf{c}_3|$. During the rest of its path the particle returns via $\mathbf{x}_1$ to $\mathbf{x}_0$, and thus backscatters. This system of equations for three unknowns yields an analytic expression that appears too lengthy to be reported here. The numerically evaluated analytic expression gives

$$W_* \approx 0.0501256. \tag{D.2}$$

Appendix E. Microscopic, mesoscopic and macroscopic scales

Eq. (14), derived in Section 4, holds for all n_x. However, different behaviors emerge for n_x belonging to different well separated scales. In such cases, different descriptions become effective. In particular, here, we use the probabilities $p^{\hookrightarrow}_k$ and $p^{\hookleftarrow}_k$ to show how different behaviors characterize three different ranges of n_x values, that we call microscopic, mesoscopic and macroscopic.

The large n_x regime, in which a Wiener process is established by properly coarse-graining, and correspondingly scaling time and space, is evidenced by the limit expressions of $p^{\hookrightarrow}_k$ and $p^{\hookleftarrow}_k$. Setting $k = \zeta n_x$, with ζ fixed in $(0, 1)$, one gets:

$$\lim_{n_x \to \infty} p^{\hookrightarrow}_k = \lim_{n_x \to \infty} p^{\hookleftarrow}_k = \lim_{n_x \to \infty} \frac{n_x - k}{n_x} = 1 - \zeta, \tag{E.1}$$

i.e. the two probabilities turn equal when $(1 - a)(1 - \zeta)n_x$ is much larger than 1, which happens sufficiently far from the left and right boundaries of the channel, where the finiteness of the medium is hardly noticed. The more correlated the process, the further away from the boundaries the cells must be for the equality (E.1) to hold with given

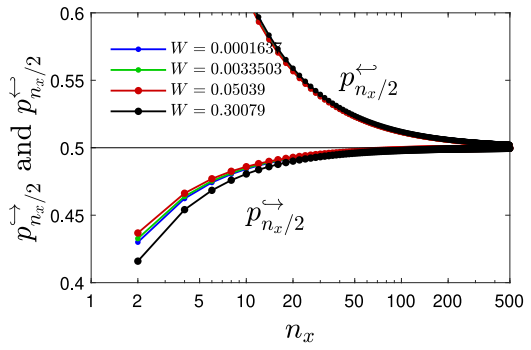

Fig. 14. Application of the CRW to the Lorentz channel. Probabilities $p^{\hookleftarrow}_{n_x/2}$ and $p^{\hookrightarrow}_{n_x/2}$, Eq. (13), versus n_x for W below and above W_*, obtained from $a(W)$ shown in Fig. 6. While $p^{\hookleftarrow}_{n_x/2}$ approaches unity at $n_x = 1$ and is quite insensitive to W, $p^{\hookrightarrow}_{n_x/2}$ increases with W for $W < W_*$ (for all n_x), and decreases with increasing W in $[W_*, W_c]$ for which results are also presented in this figure (note the ordering of the lines). Both probabilities reach 1/2 in the $n_x \to \infty$ limit in accord with Eq. (E.1) for $\zeta = 1/2$.

accuracy. Indeed, a closer to 0 or 1 requires larger n_x, at fixed ζ, for $p^{\hookrightarrow}_k$ to approach $p^{\hookleftarrow}_k$. When that condition is satisfied, in the center of the channel, $\zeta \approx 1/2$, we obtain $p^{\hookrightarrow}_k \approx p^{\hookleftarrow}_k \approx 1/2$. How large n_x and how far from the boundaries the cells have to be for an unbiased random walk to be established depends on W (Fig. 14). Given $a(W)$, the corresponding values of n_x and ζ characterize the macroscopic length scale.

Our approach allows us to characterize also the mesoscopic scale. Indeed, for given n_x and a, the conditional probabilities $p^{\hookleftarrow}_k$ and $p^{\hookrightarrow}_k$ depend linearly on k, have same slope

$$-\frac{(1-a)}{a+(1-a)n_x},$$

and decrease from values close to 1 near the left boundary of the channel, to values close to 0 near the right end of the channel. The difference between the two does not depend on k and

$$p^{\hookleftarrow}_k - p^{\hookrightarrow}_k = \frac{1}{a+(1-a)n_x} > 0, \tag{E.2}$$

because the two probabilities refer to exit to the left. The difference (E.2) is one indicator of the statistical loss of memory in the process that takes particles from cell k to the left boundary of the channel. The smaller it is, the smaller the memory of the initial state. Given any error ϵ, that can be considered negligible, we have

$$p^{\hookleftarrow}_k - p^{\hookrightarrow}_k < \epsilon \qquad \text{if} \qquad n_x > \frac{1-\epsilon a}{(1-a)\epsilon}. \tag{E.3}$$

This shows that small a, the case in which particles prefer to reverse their direction of motion, requires $n_x > 1/\epsilon$, while a close to 1 requires larger n_x, but still of order $O(1/\epsilon)$. Interestingly, even $a = 1/2$ needs large n_x: $n_x > (2/\epsilon) - 1$. Indeed, starting to move in one direction has consequences for reaching one boundary of the channel, if only a few collisions are made on average before reaching that boundary. Taking, for instance $\epsilon = 10^{-3}$, one needs more than 10^3 cells. That is why a correct assessment of finite size effects is important in the case of small systems.

Requiring $p^{\hookleftarrow}_k$ and $p^{\hookrightarrow}_k$ close to 1/2, yields the range of k values for which a coarse-grained evolution can be thought to emerge from an unbiased random walk. Taking $p^{\hookrightarrow}_{k^+} = 0.5 - \epsilon$, we obtain

$$k^+ = \left(\frac{1}{2}+\epsilon\right) n_x - \frac{a(1-2\epsilon)}{2(1-a)}, \tag{E.4}$$

while $p^{\hookrightarrow}_{k^-} = 0.5 + \epsilon$ implies:

$$k^- = \left(\frac{1}{2}-\epsilon\right) n_x - \frac{a(1+2\epsilon)}{2(1-a)}. \tag{E.5}$$

Because $p^{\hookrightarrow}_k$ decreases linearly in k, the range $k \in [k^-, k^+]$, which is about the center of the channel if n_x is sufficiently large, corresponds to values $p^{\hookrightarrow}_k$ that differ no more than the small number ϵ from 1/2. Naturally, we must have $k^- > 0$, and that means

$$n_x > \left(\frac{1+2\epsilon}{1-2\epsilon}\right) \frac{a}{1-a} \approx \frac{a}{1-a}, \tag{E.6}$$

which is a minimal requirement, surely verified if n_x obeys Eq. (E.3). For $n_x = 1/\epsilon$, the width of the interval $[k^-, k^+]$ results

$$k^+ - k^- = 2\epsilon\left(n_x + \frac{a}{1-a}\right) = 2 + \frac{2\epsilon a}{1-a}, \tag{E.7}$$

which is quite unsatisfactory, although the mesoscopic stochastic process is justified with such values of n_x. The macroscopic scale requires quite larger n_x. For instance, taking $n_x = O(1/\epsilon^2)$ yields

$$p^{\hookleftarrow}_k - p^{\hookrightarrow}_k = \frac{\epsilon^2}{\epsilon^2 a + 1 - a} = O\left(\epsilon^2\right) \tag{E.8}$$

within a range k of width $O(1/\epsilon)$. A difference $(p^{\hookleftarrow}_k - p^{\hookrightarrow}_k)$ equal or smaller than order $O(\epsilon)$, considered sufficient for the Markov process to be established, holds instead in a range of width $O(1/\epsilon^2)$. This explains, for our models, why the macroscopic scale is much larger than the mesoscopic scale, which is in turn much larger than the microscopic scale. When such separation of scales is not realized, it becomes necessary to properly quantify the finite size effects, as we have done in the present paper.

Data availability

Data will be made available on request.

References

[1] H.A. Lorentz, The motion of electrons in metallic bodies I, Proc. R. Acad. Sci. Neth. 7 (1905) 438–453.
[2] H.A. Lorentz, The motion of electrons in metallic bodies II, Proc. R. Acad. Sci. Neth. 7 (1905) 585–593.
[3] H.A. Lorentz, The motion of electrons in metallic bodies III, Proc. R. Acad. Sci. Neth. 7 (1905) 684–691.
[4] L. Rondoni, E. Cohen, On some derivations of irreversible thermodynamics from dynamical systems theory, Phys. D 168 (2002) 341–355.
[5] E. Cohen, L. Rondoni, Particles, maps and irreversible thermodynamics, Phys. A 306 (2002) 117–128.
[6] Y.G. Sinai, Dynamical systems with elastic reflections, Russian Math. Surveys 25 (2) (1970) 137.
[7] L.A. Bunimovich, Y.G. Sinai, Statistical properties of Lorentz gas with periodic configuration of scatterers, Comm. Math. Phys. 78 (4) (1981) 479–497.
[8] J. Machta, R. Zwanzig, Diffusion in a periodic Lorentz gas, Phys. Rev. Lett. 50 (1983) 1959.
[9] L.A. Bunimovich, Y.G. Sinai, N.I. Chernov, Statistical properties of two-dimensional hyperbolic billiards, Russian Math. Surveys 46 (4) (1991) 47.
[10] G.P. Morris, L. Rondoni, Periodic orbit expansions for the Lorentz gas, J. Stat. Phys. 75 (1994) 553–584.
[11] B. Moran, W.G. Hoover, S. Bestiale, Diffusion in a periodic Lorentz gas, J. Stat. Phys. 48 (1987) 709–726.
[12] J. Lloyd, M. Niemeyer, L. Rondoni, G.P. Morriss, The nonequilibrium Lorentz gas, Chaos 5 (3) (1995) 536–551.
[13] R. Klages, C. Dellago, Density-dependent diffusion in the periodic Lorentz gas, J. Stat. Phys. 101 (1) (2000) 145–159.
[14] C.P. Dettmann, Diffusion in the Lorentz gas, Commun. Theor. Phys. (Beijing) 62 (4) (2014) 521.
[15] P.M. Bleher, Statistical properties of two-dimensional periodic Lorentz gas with infinite horizon, J. Stat. Phys. 66 (1992) 315–373.
[16] J. Vollmer, L. Rondoni, M. Tayyab, C. Giberti, C. Mejía-Monasterio, Displacement autocorrelation functions for strong anomalous diffusion: A scaling form, universal behavior, and corrections to scaling, Phys. Rev. Res. 3 (1) (2021) 013067.
[17] P. Gaspard, S.A. Rice, Scattering from a classically chaotic repellor, J. Chem. Phys. 90 (4) (1989) 2225–2241.
[18] P. Gaspard, J.R. Dorfman, Chaotic scattering theory, thermodynamic formalism, and transport coefficients, Phys. Rev. E 52 (4) (1995) 3525.
[19] P. Gaspard, Chaos, Scattering and Statistical Mechanics, Cambridge University Press, Cambridge, U.K., 2010.
[20] L.A. Bunimovich, Y.G. Sinai, N.I. Chernov, Markov partitions for two-dimensional hyperbolic billiards, Russian Math. Surveys 45 (3) (1990) 105.

[21] P. Cvitanovic, R. Artuso, R. Mainieri, G. Tanner, G. Vattay, N. Whelan, A. Wirzba, Chaos: Classical and Quantum, Vol. 69, ChaosBook.org, Niels Bohr Institute, Copenhagen, 2005, p. 25.
[22] R. Zwanzig, Nonequilibrium Statistical Mechanics, Oxford University Press, Oxford, U.K., 2001.
[23] N. Chernov, R. Markarian, Chaotic Billiards, in: Mathematical Surveys and Monographs, vol. 127, American Mathematical Society, Rhode Island, United States, 2006.
[24] N. Chernov, Statistical properties of the periodic Lorentz gas. Multidimensional case, J. Stat. Phys. 74 (1994) 11–53.
[25] H. Holden, R. Piene, The Abel Prize 2013–2017, Springer, Berlin, 2019.
[26] N. Chernov, H.-K. Zhang, Billiards with polynomial mixing rates, Nonlinearity 18 (4) (2005) 1527.
[27] N. Chernov, H.K. Zhang, Improved estimates for correlations in billiards, Comm. Math. Phys. 277 (2008) 305–321.
[28] H. Larralde, F. Leyvraz, G. Martinez-Mekler, R. Rechtman, S. Ruffo, Transmission and scattering of a Lorentz gas on a slab, Phys. Rev. E 58 (1998) 4254.
[29] R. Klages, N. Korabel, Understanding deterministic diffusion by correlated random walks, J. Phys. A 35 (2002) 4823–4836.
[30] P. Gaspard, S.A. Rice, Semiclassical quantization of the scattering from a classically chaotic repellor, J. Chem. Phys. 90 (4) (1989) 2242–2254.
[31] P. Cvitanović, P. Gaspard, T. Schreiber, Investigation of the Lorentz Gas in terms of periodic orbits, Chaos 2 (1) (1992) 85–90.
[32] T. Gilbert, D.P. Sanders, Persistence effects in deterministic diffusion, Phys. Rev. E 80 (2009) 041121.
[33] T. Gilbert, D.P. Sanders, Diffusion coefficients for multi-step persistent random walks on lattices, J. Phys. A 43 (3) (2009) 035001.
[34] T. Gilbert, H.C. Nguyen, D.P. Sanders, Diffusive properties of persistent walks on cubic lattices with application to periodic Lorentz gases, J. Phys. A 44 (6) (2011) 065001.
[35] O. Weismantel, A.A. Galata, M. Sadeghi, A. Kröger, M. Kröger, Efficient generation of self-avoiding, semiflexible rotational isomeric chain ensembles in bulk, in confined geometries, and on surfaces, Comput. Phys. Comm. 270 (2022) 108176.
[36] F. Affouard, M. Kröger, S. Hess, Molecular dynamics of model liquid crystals composed of semiflexible molecules, Phys. Rev. E 54 (5) (1996) 5178–5186.
[37] S. Mehraeen, B. Sudhanshu, E.F. Koslover, A.J. Spakowitz, End-to-end distribution for a wormlike chain in arbitrary dimensions, Phys. Rev. E 77 (6, 1) (2008) 061803.
[38] A.J. Spakowitz, Z.G. Wang, End-to-end distance vector distribution with fixed end orientations for the wormlike chain model, Phys. Rev. E 72 (4, 1) (2005) 041802.
[39] E.N.M. Cirillo, M. Colangeli, A. Muntean, O. Richardson, L. Rondoni, Deterministic reversible model of non-equilibrium phase transitions and stochastic counterpart, J. Phys. A 53 (30) (2020) 305001.
[40] E.N.M. Cirillo, M. Colangeli, O. Richardson, L. Rondoni, Deterministic model of battery, uphill currents, and nonequilibrium phase transitions, Phys. Rev. E 103 (3) (2021) 032119.
[41] E.N.M. Cirillo, M. Colangeli, A. Di Francesco, M. Kröger, L. Rondoni, Transport and nonequilibrium phase transitions in polygonal urn models, Chaos 32 (9) (2022) 093127.
[42] E.N.M. Cirillo, M. Colangeli, M. Kröger, L. Rondoni, Nonequilibrium phase transitions in feedback-controlled three-dimensional particle dynamics, Phys. Rev. Res. 5 (2023) 043063.
[43] E.N. Cirillo, M. Colangeli, A. Di Francesco, M. Kröger, L. Rondoni, Particle traps and stationary currents captured by an active 1D model, Phys. A 642 (2024) 129763.